IgA autoantibodies demonstrate a novel mechanism of MuSK myasthenia gravis pathology

Citation:
Brain. 2025 Oct 28:awaf410. doi: 10.1093/brain/awaf410. Online ahead of print.

IgA autoantibodies demonstrate a novel mechanism of MuSK myasthenia gravis pathology

Gianvito Masi,[1,2] Kangzhi Chen,[1,3] Alexandra C. Bayer,[1,2] Rafael Bayarri-Olmos,[2] Minh C. Pham,[1,2] Annabel Wallace,[4] Silvia Falso,[5] Amelia Evoli,[5] Raffaele Iorio,[5] Kenneth B. Hoehn,[6] Akiko Iwasaki,[2,7,8] Richard J. Nowak[1] and Kevin C. O'Connor[1,2]

Abstract

Patients with muscle-specific tyrosine kinase (MuSK) myasthenia gravis (MG) develop muscle weakness due to functionally monovalent IgG4 autoantibodies (Abs) that target MuSK and disrupt acetylcholine receptor (AChR) clustering. Emerging evidence from other autoimmune conditions suggests that Abs of the IgA class — the archetypal immunoglobulin isotype at mucosal sites — may synergize with IgG Abs, contributing to pathology. In MuSK MG, however, the presence of disease-specific IgA Abs has not yet been recognized, limiting a broader understanding of IgG4-driven autoimmunity. To address this knowledge gap, we leveraged cell-based binding assays, patient-derived recombinant monoclonal autoantibodies (mAbs), high-throughput B-cell receptor sequencing, C2C12 mouse myotube cultures, and passive immunization experiments.

Among 112 sera collected from 25 patients with MuSK MG (discovery cohort), MuSK-specific IgA Abs were detected in eight samples, corresponding to 3/25 (12%) patients. This finding was validated in a second, independent cohort (validation cohort; n=14 individuals), wherein one additional patient (1/14; 7.1%) harbored MuSK IgA Abs. Across all cases, MuSK IgA Abs coexisted with MuSK IgG Abs, while domain-mapping demonstrated a polyclonal IgA response in 2/4 (50%) patients. Notably, in a paradigmatic case with longitudinal samples spanning over a decade, MuSK IgA seropositivity was persistent, and clonally expanded MuSK IgA B cells showed remarkable resistance to therapeutic B-cell depletion.

We generated three patient-derived MuSK-specific IgA mAbs for in-depth molecular profiling. These mAbs were highly hypermutated, bound to distinct MuSK domains, and shared target epitopes with MuSK IgG4 mAbs. Two IgA mAbs cross-reacted with murine MuSK, enabling functional studies with C2C12 myotubes. Mechanistically, individual IgA mAbs promoted AChR clustering (indicative of MuSK agonism) and partially antagonized the pathogenic effects of

MuSK IgG4 monovalency. When modeling a polyclonal response, however, the combination of the same IgA mAbs significantly impaired cluster formation, demonstrating cooperative pathogenic potential. Consistent with this, passive transfer of both IgA clones into mice induced a myasthenic phenotype characterized by progressive weight loss, muscle weakness, and structural disruption of the neuromuscular junction (effects similar to those elicited by a functionally monovalent MuSK IgG4 mAb).

These findings uncover a previously unrecognized pathogenic Ab isotype in a subset of patients with MuSK MG and show a mechanism through which bivalent MuSK Abs may synergize to induce pathology. The identification of MuSK-specific IgA B cells could signal a role of mucosal or environmental factors in the pathogenesis of MuSK MG and other IgG4-mediated diseases, offering a worthy avenue for future research.

Author affiliations:

1 Department of Neurology, Yale School of Medicine, New Haven, CT 06511, USA

2 Department of Immunobiology, Yale School of Medicine, New Haven, CT 06510, USA

3 Department of Neurology, Xiangya Hospital, Central South University, Changsha, Hunan, 41008, China

4 Yale College, New Haven, CT 06511, USA

5 Department of Neuroscience, Università Cattolica del Sacro Cuore, Rome 00168, Italy

6 Department of Biomedical Data Science and Dartmouth Cancer Center, Geisel School of Medicine at Dartmouth, Hanover, NH 03756, USA

7 Center for Infection and Immunity, Yale School of Medicine, New Haven, CT 06510, USA

8 Howard Hughes Medical Institute, Chevy Chase, MD 20815, USA

Correspondence to: Kevin C. O'Connor, PhD

Yale School of Medicine Room 353J, 300 George Street, New Haven, CT 06511, USA

E-mail: kevin.oconnor@yale.edu

Correspondence may also be addressed to: Gianvito Masi, MD

Yale School of Medicine, Room 353C, 300 George Street, New Haven, CT 06511, USA
gianvito.masi@yale.edu

Running title: Pathogenic MuSK-specific IgA antibodies

Keywords: myasthenia gravis; muscle-specific tyrosine kinase; B cells; IgA; IgG4; monoclonal autoantibodies

Introduction

Autoimmune myasthenia gravis (MG) is a rare autoantibody (Ab)-mediated neurologic condition that manifests with fluctuating muscle weakness and fatigability.[1,2] Immunoglobulin G (IgG) Abs that recognize the muscle-specific tyrosine kinase (MuSK) are found in 5-10% of patients with MG.[2-4] Compared to the most prevalent MG subtype — wherein Abs target the muscle nicotinic acethlycholine receptor (AChR) — MuSK MG is more commonly characterized by prominent bulbar weakness and shows favorable response to anti-CD20 B-cell depletion.[5,6] Indeed, following therapeutic administration of rituximab (RTX), an anti-CD20 chimeric monoclonal antibody (mAb), most patients achieve clinical remission and show a marked reduction in their MuSK IgG titers.[7-12]

From an immunological perspective, and in contrast with the IgG1-2-3-driven AChR MG pathology, the autoimmune response occurring in MuSK MG is dominated by IgG4, an antibody isotype with unique molecular properties.[13-15] Because of specific amino acid residues in the heavy-chain constant region, IgG4 is less effective at activating complement or engaging with effector cells compared to other IgG subclasses. Furthermore, circulating IgG4 antibodies stochastically exchange half-molecules with other unrelated IgG4, becoming bispecific and unable to cross-link target antigens, a process known as fragment antigen binding (fab)-arm exchange (FAE).[16,17] These “anti-inflammatory” features notwithstanding, in vitro and in vivo studies support a direct, prominent role of IgG4 Abs in MuSK MG pathogenesis.[3,18-21]

At the neuromuscular junction (NMJ), MuSK interacts with the agrin/low-density lipoprotein receptor-related protein 4 (LRP4) complex and orchestrates a signaling cascade that promotes aggregation of AChR on the muscle endplate, contributing to NMJ development/maintenance and effective neuromuscular transmission.[22-24] In MuSK MG, however, IgG4 Abs (which comprise more than 90% of circulating MuSK IgG) sterically block the interaction between MuSK and LRP4, thus hindering MuSK activation and its intracellular signaling cascade.[13,25] This event ultimately leads to the impairment of AChR clustering and the failure of neuromuscular transmission.

The role of the less abundant MuSK-specific IgG1, 2, and 3 Abs is still under investigation, but cumulative evidence suggests that their mechanism of action differs from that of IgG4 Abs. Unlike IgG4 Abs that are functionally monovalent due to FAE, IgG1-3 MuSK Abs are bivalent and have the potential to force-dimerize MuSK and activate its signaling cascade. Indeed, studies on MuSK-specific mAbs have demonstrated the capacity of bivalent clones to induce MuSK phosphorylation and agrin-independent activation of the AChR clustering pathway.[21,26,27] Differences in Ab valency seem to dictate divergent functional effects in vivo as demonstrated by a passive transfer experiment in which bispecific, monovalent IgG4 mAbs induced severe and rapid myasthenic symptoms in mice, while injection of the same clones as bivalent antibodies led to absent or milder pathogenic effects.[28] In a recent study, however, IgG4-depleted pooled sera induced MuSK, DOK7, and βAChR phosphorylation in vitro, but cluster formation was impaired, mirroring the detrimental effects induced by IgG4 Abs.[29] A crucial difference between these investigations lies in the experimental approach of testing single mAbs versus polyclonal sera.

Beyond IgG4 Abs and the smaller population of IgG1-3 Abs, whether immunoglobulins of other isotypes play a role in the autoimmune response against MuSK remains unclear. Growing evidence from other autoimmune conditions suggests that IgA, an antibody isotype that dominates mucosal immune responses and the second-most prevalent isotype in serum, may synergize with IgG and contribute to pathology.[30,31] In MuSK MG, however, data regarding the presence and role of IgA

Abs are lacking, limiting a broader understanding of the mechanisms that govern IgG4-mediated autoimmunity.[32]

In this study we show that a subset of patients with MuSK MG harbors IgA Abs coexisting with IgG Abs. Functional profiling of patient-derived MuSK-specific IgA mAbs revealed divergent mechanistic properties depending on the experimental context. Individual IgA mAbs activated MuSK signaling and partially rescued the dispersal of AChR clusters induced by pathogenic IgG4 Abs. In sharp contrast, combining two IgA clones (an experiment designed to mimic serum polyclonality) led to striking impairment of AChR clustering and triggered myasthenic symptoms in passively immunized mice. Collectively, this study identifies a novel MuSK MG Ab isotype with demonstrated pathogenic capacity and highlights a previously unappreciated potential link between mucosal triggers and MuSK autoimmunity.

Material and methods

Detailed methods are described in the **Supplementary material**.

Results

MuSK IgA Abs are found in a subset of patients with MuSK MG

To measure MuSK-specific IgA Abs in serum, we optimized a live, MuSK-expressing cell-based assay (CBA) using flow cytometry.[20] First, we validated the specificity of a commercial anti-IgA secondary antibody using MuSK1B,[20] a patient-derived MuSK-specific IgG3 mAb that was subcloned into expression vectors encoding the heavy chain constant regions of the four IgG subclasses (IgG1, 2, 3 and 4), IgA1 (the predominant IgA subclass in serum), and IgM. As expected, the anti-IgA secondary antibody recognized MuSK1B subcloned into the IgA1 backbone but did not show IgG or IgM cross-reactivity (**Fig. 1A**). Serological assays that measure IgA (and IgM) can show non-specific background signal especially when certain antigens are expressed at

high density on cells.[32] Thus, we conducted a series of preliminary experiments in which we tested representative sera from patients with MuSK MG and controls (healthy individuals and AChR MG patients) using increasing serum dilutions. Based on these tests, a 1:100 dilution factor yielded an optimal signal-to-noise ratio that increased the assay specificity without reducing its sensitivity.

In the initial MuSK IgA screening, we included a total of 112 longitudinally collected sera derived from 25 patients (discovery cohort) with a clinical and laboratory-confirmed diagnosis of MuSK MG, as well as 30 sera from healthy donors (HD) and 32 sera from patients with AChR MG. Based on the positivity cutoff determined by the HD group, eight out of 112 MuSK MG sera, corresponding to 3/25 unique patients (12%), were positive for MuSK IgA Abs (**Fig. 1B**). To validate our findings in an independent cohort, we screened an additional 23 sera from 14 patients with MuSK MG (validation cohort) and identified one patient with four longitudinally collected sera harboring MuSK IgA Abs (**Fig. 1C**). Collectively, MuSK IgA Abs were detected in 12 out 135 (8.9%) tested sera and 4/39 (10.3%) patients with MuSK MG. Flow cytometry testing of an additional 112 control sera from patients with other neurologic disorders — AChR MG, neuromyelitis optica spectrum disorder, and myelin oligodendrocyte glycoprotein antibody-associated disorder (MOGAD) — identified one sample from a MOGAD patient exhibiting low positivity (1/112, 0.9%). In this case, IgA binding was restricted to cells expressing high membrane densities of MuSK (MuSK-GFP high) **(Supplementary Fig.1A-C)**. Conversely, across all MuSK MG sera, IgA Abs recognized MuSK irrespective of its expression level. Thus, a threshold of MuSK cell density discriminated IgA Abs in MuSK MG patients from a disease control, probably reflecting qualitative differences in the binding capacity of the detected Abs (**Supplementary Fig.1D**).

In the two MuSK MG cohorts, MuSK IgA Abs were always co-detected with MuSK IgG Abs (representative fluorescence microscopy images are shown in **Fig. 1D**), but no association was found between IgA and IgG Abs' levels measured by flow cytometry (**Fig. 1E**). Previous studies have demonstrated a good correlation between disease status and MuSK IgG (and IgG4) levels.[12,33,34] In our cohort, MuSK IgG —but not IgA—levels moderately correlated with disease severity at sampling (**Supplementary Fig. 2A**). Estimation of absolute MuSK IgG4 and IgA titers

by flow cytometry showed an IgG4 predominance in most cases, confirming the primary role of IgG4 Abs in the disease (**Supplementary Fig. 2B**). Demographic and clinical data of the four MuSK IgA seropositive patients (MuSK-1, MuSK-2, MuSK-3, and MuSK-4) are summarized in **Supplementary Table 1**. No significant differences were identified when comparing the clinical features of these patients with those who were seronegative for MuSK IgA Abs (**Supplementary Table 2**). In addition, we reviewed corresponding clinical records to investigate factors (including documented infections and immunizations) potentially influencing the production of MuSK IgA Abs, but the clinical histories of the four patients were unrevealing in this regard.

For three MuSK IgA seropositive patients, longitudinal samples were available, which allowed us to track their Abs levels over time. In the case of MuSK-2, a patient with three consecutive sampling timepoints, MuSK IgA Abs were detected only in the first sample collection. In MuSK-4, instead, four longitudinal samples collected within the first year of symptom onset were positive for MuSK IgA Abs (**Supplementary Fig. 3**). In the third patient (MuSK-1), fourteen serum samples were available, spanning almost twelve years (140 months) of disease, and within this timeframe RTX was administered six times to treat or prevent clinical relapses (**Fig. 1F**). Notably, while MuSK IgG Abs were detected at all timepoints, MuSK IgA Abs were first detected at month 61 of the serial collection (9^{th} sampling timepoint) without evidence of preceding infections or vaccinations, and this IgA response persisted for nearly 7 years, up to the last available sample. Both MuSK IgG and IgA levels diminished following each RTX cycle, but the magnitude of reduction was greater for IgG than for IgA (11^{th}-12^{th} timepoint: -66.4% vs. -13.2%; 13^{th}-14^{th} timepoint: -88.8% vs. -43.86%) (**Fig. 1G**). Taken together, these data show that (1) a subset of patients with MuSK MG harbors MuSK IgA Abs coexisting with MuSK IgG Abs; (2) MuSK IgA Abs can be detected in both early and advanced stages of the disease; (3) both MuSK IgA and IgG Ab levels decline following RTX administration, albeit with different proportions, suggesting that MuSK-specific IgA and IgG-producing B cells may differ in their susceptibility to anti-CD20 depletion.

Patient-derived MuSK-specific IgA mAbs have heterogenous properties

To examine the molecular and functional features of MuSK IgA Abs and compare them to those of MuSK IgG4 Abs, we leveraged a B-cell culturing approach through which we previously generated human-derived IgG mAbs from patients with MuSK and AChR MG.[20,35,36] Patient $CD27^+$ B cells were cultured in 96 well-plates and differentiated in antibody-secreting cells. Following a high-throughput screening of B cell supernatants, the B cells from those wells containing MuSK IgA Abs were cloned to obtain recombinant mAbs. Based on the number of CD27+ B cells isolated from each patient, the frequency of circulating MuSK IgA B cells was 0.01% (3 cells) for patient MuSK-1, 0.001% (1 cell) for patient MuSK-2, 0.012% (2 cells) for patient MuSK-3. Similar frequencies were observed in a parallel MuSK IgG screening (**Supplementary Table 3**), further confirming the exceptional rarity of blood-derived MuSK-specific clones.[20,21,35,37] Using this culturing strategy, we generated three MuSK-specific IgA mAbs (referred to as aMu1, aMu2, and aMu3), each derived from a distinct MuSK IgA seropositive patient (MuSK-1, MuSK-2, MuSK-3). In this nomenclature, "a" denotes the Ab isotype (IgA), and "Mu" refers to MuSK. Immunoglobulin subclass PCR showed that all three mAbs derived from IgA1-expressing B cells; accordingly, an IgA1 recombinant expression vector was used for the expression of these three MuSK IgA mAbs unless otherwise indicated. In humans, serum IgA is chiefly monomeric, whereas secretory IgA is mainly dimeric.[38] In line with this, no evidence of dimeric MuSK IgA Abs was found by testing patients' sera (**Supplementary Fig. 4**), suggesting that the majority of circulating MuSK IgA Abs exist as monomers. Therefore, the recombinant IgA mAbs were expressed in a monomeric form.

First, we confirmed the specificity of the newly generated IgA mAbs by live CBA, using both flow cytometry and fluorescence microscopy. The three IgA mAbs bound to full-length human MuSK over a wide range of concentrations, and their relative binding strength was comparable to that of MuSK1B, a control mAb with subnanomolar affinity for MuSK (**Fig. 2A**).[39] Confocal fluorescence microscopy demonstrated a clear membrane staining and selective labeling of MuSK-expressing cells (**Fig. 2B**), whereas cross-reactivity with two clinically relevant neurologic autoantigens, AChR and myelin oligodendrocyte glycoprotein (MOG), was not observed (**Supplementary Fig.**

5). V(D)J sequencing analysis showed that the three mAbs were heavily somatically hypermutated, with an average V gene amino acid replacement mutation frequency of 19.5 ± 5.2% and 13.9 ± 3.4% (mean ± SD) for the heavy and light chains, respectively (**Table 1**). Two N-linked glycosylation sites—a feature of many MuSK IgG4 mAbs[40,41]— were found in aMu1 (both encoded by germline-derived nucleotides in the VH4-34 gene), but not in the other two IgA mAbs.

MuSK is a tyrosine kinase receptor comprised of three immunoglobulin (Ig)-like domains, one Frizzled-like (Fz-) domain, and an intracellular kinase domain.[42-44] Most (if not all) patients with MuSK MG harbor IgG Abs that recognize the Ig-like 1 domain.[19] Conversely, IgG Abs targeting other MuSK domains are found less frequently.[45] To determine the domain specificity of the three IgA mAbs, we performed an experiment in which—as we previously demonstrated—each mAb is tested for binding to single MuSK domains.[20] Using this strategy, we determined that aMu1, aMu2, aMu3 recognized the Ig-like 1, the Fz-, and Ig-like 2 domain, respectively (**Fig. 2C**). Because MuSK IgA and IgG Abs coexist in sera, and IgG4 is the predominant IgG subclass in MuSK MG, we then asked whether the IgA mAbs could compete with IgG4 Abs for MuSK binding. To this end, we employed three IgG4 mAbs that were characterized in previous studies: MuSK1A which recognizes the Ig-like 2 domain, and 6C6 and 2E6 both targeting the Ig-like 1 domain.[20,35] After incubating MuSK-expressing cells with an IgA mAb in excess, an IgG4 mAb was added and detected by flow cytometry using an experimentally validated anti-IgG Fcγ secondary antibody (**Fig. 1A**). In these experiments, pre-incubation with aMu1 IgA reduced the detection of 2E6 IgG4 by 93.0 %, while aMu3 IgA hindered binding of MuSK1A IgG4 by 92.6% (**Fig. 2D**).

In summary, we successfully generated three patient-derived MuSK-specific IgA1 mAbs from the $CD27^+$ memory B-cell compartment. These mAbs show the hallmarks of affinity maturation, target three different MuSK domains, and exhibit competitive binding with patient-derived IgG4 Abs, suggesting identical or partially overlapping target epitopes (**Fig. 2E**). Given the competitive binding, we asked whether high titers of MuSK IgG4 Abs could have hindered the detection of MuSK IgA Abs in the screening CBA. To address this, we depleted IgG from MuSK IgG-positive sera in the discovery cohort and tested the IgG-negative fractions by CBA. No additional MuSK-IgA positive samples were identified following IgG removal, indicating that the CBA provided

sufficient antigen density to allow parallel detection of both IgA and IgG Abs (**Supplementary Fig. 6**).

High-throughput B-cell receptor sequencing identifies RTX-resistant MuSK-specific IgA clones

We previously demonstrated that MuSK-specific IgG4 B cells can resist RTX and reemerge into circulation prior to relapses.[35] We next sought to verify whether MuSK-specific IgA B cells exhibit a similar behavior. We queried B-cell receptor (BCR) repertoire libraries previously generated through either bulk or single-cell sequencing of samples derived from patient MuSK-1, from whom aMu1 IgA mAb was cloned (**Supplementary Table 1**).[35] Additionally, we performed bulk BCR sequencing on newly collected samples belonging to patients MuSK-1 and MuSK-2 (the latter patient was the source of aMu2 IgA mAb). B-cell clones and clonal variants —cells that originate from a common V(D)J rearrangement—were identified by clustering BCR heavy chain sequences by sequence similarity. Based on this search, we found 24 distinct clonal variants of aMu1, belonging to five different timepoints that spanned over six years of disease (**Fig. 3A-B**). In addition, one clonal variant of aMu2 was found in the same timepoint from which aMu2 was generated (**Supplementary Fig. 7**). Clonal variants of aMu1 were detected before and after multiple RTX cycles. Nine clonal variants (7-11; 21-24) were found in PBMC samples collected within three months after RTX administration, indicating remarkable resistance to anti-CD20 B-cell depletion (**Fig. 3A**). All variants were highly mutated, with between 12.6 and 24.2% nucleotide difference from their predicted unmutated V gene (**Fig. 3B**). Further, the mean of somatic hypermutations in this lineage was significantly positively correlated with sample time (slope=0.79 mutations/month, date randomization $p=4x10^{-5}$), indicating that this lineage is measurably evolving and likely undergoing additional affinity maturation during its 77 month sampled period.[46] Five representative clonal variants, corresponding to the earliest detection of MuSK IgA in serum, were expressed, and their specificity was confirmed by CBA (**Fig. 3C**). Notably, all clonal variants were IgA, and thus evidence of MuSK IgA-IgG class-switch events was not observed.

Individual IgA mAbs can behave as MuSK agonists and functionally antagonize IgG4 pathogenic monovalency in vitro

Because bivalent MuSK IgG mAbs have previously shown agonistic potential by inducing varying degrees of MuSK phosphorylation and AChR clustering,[27] we reasoned that the IgA mAbs could exhibit a similar behavior. To test this hypothesis, we cultured C2C12 myotubes which have the key signaling machinery, except neuronal agrin, to form AChR clusters. Treatment with agrin activates the LRP4-MuSK-DOK7 pathway and leads to the formation of AChR clusters (modelling nascent NMJs), which can be readily visualized and quantified using fluorescently labeled alpha bungarotoxin. Crucially, the addition of functionally monovalent MuSK IgG4 Abs blocks MuSK-LRP4 interaction and hampers cluster formation.

To assess whether the MuSK IgA mAbs could elicit AChR clustering independent of agrin, we incubated fully differentiated myotubes with the IgA mAbs in the absence of agrin and counted the number of "mature" ($\geq$ 15 μm^2) AChR clusters.[27] 8-18C5 IgA, a mAb that binds to MOG,[47] showed no conspicuous effect on clustering level (**Fig. 4A**). In sharp contrast, both aMu1 and aMu3 increased the number of AChR clusters, achieving 57.9% and 40.3% of the agrin effect, respectively ($p<0.0001$ compared to 8-18C5). A modest increase in clusters, albeit not statistically significant, was also observed with aMu2, the IgA mAb specific for the Fz-domain. Further corroborating the agonistic potency of aMu1 and aMu3, immunoblotting showed that both mAbs induced MuSK phosphorylation, whereas aMu2 and 8-18C5 did not (**Fig. 4B**). Despite their agonistic activity, aMu1 and aMu3 moderately reduced agrin-dependent cluster formation (**Fig. 4C**), suggesting functional interference with the agrin-LRP4-MuSK pathway.

The IgA mAb aMu2, by contrast, was the only clone lacking significant agonistic activity on mouse C2C12 myotubes, which prompted us to investigate the underlying cause. Notably, sequence alignment of human and mouse MuSK demonstrates high interspecies identity (99-96%) in the Ig-like 1 and 2 domains, but reduced homology (approximately 86%) in the Fz-like domain (**Supplementary Fig. 8A**). Based on this observation, we asked whether aMu2 lacked cross-reactivity with mouse MuSK. To test this hypothesis, Ab binding to mouse MuSK was assessed

by CBA. Whereas aMu1 and aMu3 bound strongly to both human and murine MuSK, aMu2 displayed only minimal reactivity toward the murine isoform (**Supplementary Fig. 8B).** We therefore concluded that the C2C12 system could not provide a reliable assessment of aMu2's functional activity and excluded this mAb from subsequent experiments.

Because the other two mAbs, aMu1 and aMu3, exhibited agonistic potency in the C2C12 clustering experiments, we then asked whether they could antagonize the pathogenic effects of FAE MuSK IgG4 Abs and rescue cluster formation in vitro. To test this, we leveraged an established experimental approach[21,39], and employed three MuSK IgG4-derived Fabs to mimic the pathogenic properties of MuSK IgG4 functional monovalency (**Fig. 4D-F**). As expected, agrin-dependent AChR clustering was diminished by MuSK1A Fab (-98.5%), 6C6 Fab (-86.6 %), and 2E6 Fab (-46.34%).[35,39] In the presence of MuSK1A Fab, both aMu1 and aMu3 partially rescued AChR clustering (respective increases of +44.5%; $p< 0.0001$, and +45.1%; $p<0.0001$, compared to the "Fab plus agrin" condition). In a similar pattern, when co-incubated with 6C6 Fab, aMu1 and aMu3 increased the number of AChR clusters (respective increases of +32.6%, $p< 0.0001$; +31.6%, $p<0.001$). No differences, however, were observed upon treatment with Fab 2E6, the Fab with the least pathogenic capacity among the three, as the addition of the IgA mAbs did not significantly change the number of clusters. These findings confirmed that, similar to bivalent IgG, individual MuSK IgA Abs can exhibit both agrin-independent agonistic activity and the potential to antagonize functionally monovalent IgG4 Abs.

The combination of two IgA mAbs potently inhibits AChR cluster formation despite persistent MuSK phosphorylation

Multiple lines of evidence suggest that the production of MuSK IgG is polyclonal: clonally-unrelated IgG mAbs have been generated from single individuals, and circulating IgG Abs in a given patient can target different MuSK domains.[20,21,45] To investigate whether polyclonality is also a feature of circulating MuSK IgA Abs, we tested representative sera from the MuSK IgA-seropositive patients, leveraging the same domain-mapping strategy that was previously employed

for the mAbs. In two patients (MuSK-1 and MuSK-3) we detected IgA Abs against a single domain (the Ig-like 1 and Ig-like 2 domains, respectively), whereas in sera from MuSK-2 and MuSK-4, the IgA Abs recognized two or three MuSK domains, indicative of a polyclonal response (**Fig. 5A**).

This finding prompted us to assess how the simultaneous action of multiple IgA mAbs can affect AChR clustering. We therefore tested the combination of aMu1 and aMu3 on C2C12 myotubes and counted the number of clusters (**Fig. 5B**). Contrary to expectations, in the absence of agrin the two mAbs did not exert an additive or synergistic effect on cluster formation but, rather, we found very few clusters, with a clustering level comparable to that of a non-binding control mAb ($p>0.99$ compared to 8-18C5) (**Fig. 5C**). Moreover, this combination potently inhibited agrin-dependent AChR clustering to a greater extent than either mAb alone, achieving ~90% reduction in clusters compared to agrin (**Fig. 5D**). This inhibitory effect required the simultaneous action of two mAbs exhibiting MuSK specificity, because pairing either clone with an irrelevant IgA mAb (such as the MOG-specific 8-18C5) did not replicate the result (**Fig. 5C-D**). Despite this impairment of clusters, immunoblotting confirmed that the combination of aMu1 and aMu3 retained the capacity to induce MuSK phosphorylation (**Supplementary Fig. 9**). Collectively, these data indicate a complex interplay between Ab clonality and MuSK signaling. Indeed, single IgA mAbs activated MuSK (thereby promoting cluster formation) while partially inhibiting agrin activity. Instead, the combination of two IgA mAbs failed to sustain cluster formation and, at the same time, strongly antagonized agrin-mediated clustering. Thus, the simultaneous engagement of MuSK by two IgA mAbs was responsible for enhanced pathogenic effects in vitro.

Passive transfer of patient-derived MuSK IgA mAbs induces a myasthenic phenotype in mice

Finally, to investigate the pathogenic potential of MuSK IgA Abs in vivo, we established a passive immunization MG model. In a previous study, intraperitoneal (IP) injections of functionally monovalent IgG4 MuSK-specific mAbs binding to the Ig-like 1 domain induced progressive

muscle weakness in immune-deficient NOD-SCID mice.[28] Thus, as proof of concept, we first tested MuSK1A, a patient-derived MuSK IgG4 mAb binding to the Ig-like 2 domain (**Supplementary Figure 10A**).[20] To emulate the monovalency of IgG4 Abs, we generated a bispecific mAb using a controlled FAE process.[48] The resulting mAb binds to MuSK with one arm, while the second antibody arm recognizes the keyhole limpet hemocyanin (KLH). In alignment with the findings achieved with two other MuSK IgG4 clones (13-3B5 and 11-3F6),[28] mice receiving three IP injections of MuSK1A-KLH (1 mg/kg on day 0, 3 and 6) showed overt signs of muscle weakness within one week of treatment, whereas two control groups (untreated mice and mice receiving a KLH IgG mAb) remained unaffected (**Supplementary Fig. 10B-E**). Notably, a decline in body weight was observed in mice treated with MuSK1A-KLH, likely due to the decreased ability to reach water and food and the prominent vulnerability of bulbar muscles to MuSK Abs.[5,49]

After confirming the pathogenic capacity of a human-derived IgG4 mAb in our model, we next sought to evaluate the effects of MuSK IgA Abs. Because in immune-deficient mice the half-life of adoptively transferred IgA is relatively shorter than that of IgG (15-22 hours vs. 2-3 days),[50] we implemented a daily passive transfer protocol to ensure continuous in vivo IgA exposure. Additionally, to emulate the polyclonal IgA profile observed in patients, we treated mice with a 1:1 mixture of two MuSK IgA mAbs (aMu1 and aMu3, 5 mg/kg total) (**Fig. 6A**). This regimen caused progressive weight loss, with a 20% reduction in body weight on day 9 compared to baseline (**Fig. 6B**). Signs of muscle weakness emerged after one week of treatment, as shown by a significant decrease in grip strength on day 9 (-31.7%, p=0.0079, compared to mice receiving an equivalent daily dose of KLH IgA) (**Fig. 6C**), and shorter hanging times — assessed using two approaches (-71% in both tests, p=0.0079) (**Fig. 6D-E**). At the end of the experiment, sera collected from mice exhibiting muscle weakness confirmed the presence of circulating MuSK-specific IgA Abs (**Fig. 6F**), and whole-mount immunostaining of the epitrochleoanconeus (ETA) — a fast-twitch muscle in the upper forelimb, distal from the injection site — demonstrated IgA deposition at the NMJs (**Fig. 6G**). In sharp contrast to the intact, pretzel-like morphology of healthy NMJs observed in the KLH IgA group, the NMJs of MuSK IgA-treated mice lost their complex architecture and appeared fragmented (**Fig. 6H**). In sum, passive transfer of two patient-derived

MuSK IgA mAbs induced a myasthenic phenotype in mice, demonstrating the pathogenic capacity of MuSK IgA in vivo.

Discussion

The detection of MuSK-specific IgG Abs represents the diagnostic hallmark of MuSK MG. Here we showed that, beyond Abs of the IgG isotype, approximately 10% of MuSK MG patients harbor MuSK IgA Abs and that these Abs have pathogenic potential in vivo. Our data contribute to the otherwise limited evidence suggesting a role for IgA Abs in neurologic autoimmunity. In N-methyl-D-aspartate receptor (NMDAR) encephalitis, for example, pathogenic IgG1 Abs are found in most patients but NMDAR-IgA seropositivity is enriched in those with a paraneoplastic cause, primary ovarian teratomas.[51] Histological examination of such tumors revealed germinal center-like architectures in close proximity with neuroglial tissues structures, which are potential sites for B-cell autoimmunization, affinity maturation, and class-switching.[51] NMDAR IgA Abs have also been detected in a subset of patients with slowly progressive cognitive impairment and showed pathogenic potential in vitro, wherein patients' purified IgA (but not that of controls) decreased membrane NMDAR expression in cultured neurons.[52] More recently, IgA Abs recognizing MOG have been found in patients with central nervous system demyelination, presenting with a distinct clinical phenotype, and with MOG- and aquaporin-4 IgG seronegativity.[53] Given the detection of MuSK IgA Abs in a limited number of patients, our study was not positioned to conclusively establish whether MuSK IgA Ab seropositivity correlates with specific clinical patterns; larger cohorts will be required to identify such associations. This limitation notwithstanding, we found MuSK IgA Abs in patients from two independent MG cohorts, further supporting the generalizability of our findings. Cell-based screening of individuals with other neurologic diseases (OND) identified a MOGAD sample harboring low levels of MuSK IgA Abs. Notably, two different IgA binding thresholds were observed when comparing the OND and the MuSK MG sera. This finding could signal qualitative differences (such as variations in affinity) among MuSK IgA Abs,[54] which warrants further confirmation. It is conceivable, nonetheless, that, by overexpressing MuSK, our screening method enabled detection of both low- and high-affinity IgA Abs. Low-affinity Abs, for instance, can include naturally occurring Abs (NAbs), germline-encoded immunoglobulins that are polyreactive and target conserved epitopes.[55,56] Predominantly

of the IgG and IgM isotype, NAbs also include IgA and are produced without explicit antigenic stimulation.[57] In sharp contrast to NAbs, the IgA mAbs generated from three MuSK MG patients showed a high frequency of somatic hypermutation, clear specificity for MuSK, and relative binding curves that were comparable to that of MuSK1B, an IgG4 mAb with known, high affinity for MuSK.[39] Although direct affinity measurements lie beyond the scope of this study, the molecular features of patient-derived IgA mAbs confirm the contribution of a previously unrecognized Ab isotype in the MuSK-specific repertoire.

In humans, IgA has two subclasses: IgA1 and IgA2. The three MuSK IgA mAbs were cloned from IgA1 B cells. IgA1 is the predominant IgA subclass in serum where it is mostly found in monomeric form, whereas at mucosal surfaces, secretory IgA1 and IgA2 antibodies exist as dimers, and their relative proportions vary based on the mucosal site.[58,59] While secretory IgA antibodies represent the first line of defense against toxins and pathogens invading the mucosa, the function of serum IgA is poorly understood. Serum IgA can bind to multiple receptors including the myeloid-cell-specific type I Fc receptor for IgA (FcαRI), which is expressed by neutrophils, eosinophils, monocytes, and macrophages, and it is believed to induce inhibitory signals and contribute to immune homeostasis. Of note, FcαRI has been shown to facilitate the internalization of IgA1-opsonized bacteria by hepatic Kupffer cells in a non-inflammatory context, suggesting that IgA1 antibodies represent a second mechanism of defense against intestinal bacteria that invade the portal venous system.[60] Whether MuSK IgA1 Abs can recognize bacteria or other pathogens remains undetermined; this possibility would imply molecular mimicry, a mechanism through which certain pathogens trigger the production of antibodies that, in turn, cross-react with self-proteins by virtue of structural homology.[61] Some of the strongest evidence supporting this concept comes from recent investigations on Abs in rheumatoid arthritis (RA).[62,63] Clonally related IgG and IgA Abs binding to RA-relevant autoantigens have been shown to cross-react against a gut-derived bacterial strain of *Subdoligranulum*, and mice colonized with the bacterial isolate developed arthritis with pathology similar to human RA.[62] The role (or lack thereof) of gut commensals (or other pathogens) in MuSK MG initiation and/or progression remains undetermined, but the generation of MuSK-specific IgA mAbs provides both a rationale and an unprecedented opportunity for analogous, mechanistic investigations.

Molecular and functional profiling of individual IgA mAbs showed binding to different MuSK domains, varied agonistic potencies on MuSK signaling, and functional antagonism of two IgG4-derived Fabs in vitro. The latter effect was not simply due to competitive binding for the same (or proximal) MuSK epitopes, because a partial rescue of clustering was also observed when an IgA mAb and Fab targeted different MuSK epitopes. This observation aligns with a MuSK MG mouse model in which an agonist mAb targeting the Fz-domain activated MuSK and functionally antagonized Ig-like 1 domain-specific FAE IgG4 mAbs.[64]. In addition, both aMu1 and aMu3 partially reduced AChR clustering in the presence of agrin, suggesting pathogenic potential, and their combination significantly amplified this effect. These findings share commonalities with a study in which bivalent IgG1-3 Abs from patients' pooled sera impaired AChR clustering while still activating MuSK signaling.[29] IgG1-3-mediated pathogenic effects were also observed with DOK7-overexpressing myotubes, wherein cluster formation is spontaneous and does not require agrin.[25] Because DOK7 acts downstream of MuSK, it was hypothesized that the effect of MuSK IgG1-3 Abs may not be limited to the disruption of the canonical clustering pathway.

Further details of the mechanism underpinning the detrimental effect of bivalent clones remain to be found, but our experiments indicate that polyclonality may be a key factor that amplifies the pathogenicity of bivalent Abs. In line this hypothesis, a recent investigation demonstrated induction of myasthenic symptoms in mice using a polyclonal mixture of Abs specific for the Fz-like domain.[65] It is plausible that while the pathogenic potential of single bivalent clones is counterbalanced by their agonistic capacity, the combination of two (or more) clones can override MuSK agonism, leading to overt pathogenicity. Consistent with this, in our passive immunization experiment, injection of two bivalent IgA mAbs — emulating patient polyclonal serum —induced a myasthenic phenotype in mice. A speculative working model is graphically depicted in **Fig.7**. One attractive mechanistic hypothesis is that the binding of multiple Abs could induce conformational changes that "lock" the extracellular portion of MuSK in a non-physiological configuration, hampering the subsequent formation and/or stability of AChR clusters. Indeed, a role of the MuSK ectodomain in mediating the association of MuSK with other synaptic components has been proposed.[66,67] An alternative possibility is that the activation of the MuSK

signaling cascade induced by multiple Abs stimulates a negative feedback loop, resulting in clustering impairment. In dose-response and time-course experiments performed on myotubes, however, agrin and an agonist Fz-specific mAb elicited remarkably similar phosphorylation cascades.[26] In aggregate, our findings strongly suggest that the cooperation among bivalent clones represents a novel pathogenic determinant in MuSK MG. We and others have described a similar mechanism in the context of AChR MG immunopathology wherein multiple AChR-specific clones can synergize to enhance pathogenic effects.[36,68] Future studies are warranted to elucidate the molecular and functional interactions of IgA and IgG1-3 clones in serum and to assess how these interactions affect MuSK function.

The identification of aMu1 and multiple, historic clonal variants resisting consecutive cycles of RTX generates questions regarding the phenotype of MuSK IgA B cells and the specific mechanisms that confer resistance to anti-CD20 depletion. We previously showed that short-lived plasmablasts are key IgG4 Ab-producing cells in MuSK MG and that MuSK-specific IgG4 clones can also escape depletion, reemerging into circulation prior to clinical relapse.[35,37] In the current study, appreciable differences between the kinetics of MuSK IgG and IgA levels in response to RTX suggest that IgA B cells may be less susceptible to CD20 B-cell depletion than IgG4 B cells. A "resilient" pool of circulating IgA B cells has also been described in patients with multiple sclerosis, treated with ocrelizumab.[69] Among the numerous hypotheses that can explain resistance to CD20 depletion, the most plausible explanations are the limited efficacy of the drug in targeting tissue-resident B cells or the lower expression of CD20 in residual memory B cells.[70,71] Because in humans IgA production primarily occurs in the intestinal Peyer's patches, an attractive explanation is that a subset of mucosal resident IgA B cells is self-sufficient and not replenished by $CD20^+$ B cells. Compellingly, in a study on patients with RA, the majority of circulating plasmablasts — observed during B-cell depletion —expressed IgA as well as β7 integrin and CCR10, which are receptors for mucosal homing.[72] In the same study, proliferating IgA plasmablasts, but not $CD20^+$ cells, were detected in mucosal biopsies from patients with diffuse large B-cell lymphoma treated with RTX. These data support the hypothesis that mucosal B cells can resist RTX treatment and continuously differentiate into circulating IgA-producing plasmablasts. It is tempting to speculate that RTX-resilient MuSK IgA B cells could represent an unrecognized cellular reservoir poised to perpetuate MuSK autoimmunity. It is also plausible that

MuSK IgA and IgG4 B cells respond similarly to RTX but differ in the kinetics that govern post-RTX repopulation. Future investigations will focus on the origin, location, and phenotype of such cells.

The detection of IgA Abs in an IgG4-driven disease opens new questions regarding the pathways leading to IgG4 class-switch. These are of substantial interest not only for MuSK MG but also for a better understanding of the autoimmune mechanisms underlying other IgG4-mediated conditions. Prompted by the isolation of MuSK IgA1 B cells, we analyzed bulk BCR sequencing libraries derived from two MuSK IgA-seropositive patients, but we did not find clones sharing MuSK IgA and IgG isotypes which would provide evidence for IgA-IgG class-switching events in vivo. These data align with recent findings in pemphigus vulgaris, an IgG4-mediated blistering disorder in which Abs target the adhesion proteins desmoglein (DSG) 3 and DSG1. In this condition, phylogenetic analysis combined with subclass-specific B cell deep sequencing showed that the majority of anti-DSG IgG4 B-cell clones lack relatives in other subclasses and evolve independently of IgA1.[73] Conversely, most anti-DSG IgA1 B cells demonstrated evidence of class switch from IgG1 or to IgA2.

Finally, our study has translational implications. Recent therapeutic advances for Ab-mediated autoimmune conditions include inhibitors of the neonatal crystallizable fragment receptors — such as efgartigimod and rozanolixizumab, recently approved for MG[74,75] — as well as engineered IgG-specific cleaving enzymes which are emerging as promising interventions.[76] These treatments are effective at reducing pathogenic IgG levels but do not affect other immunoglobulin isotypes. Given that MuSK IgG4 Abs were detected at higher titers compared to MuSK IgA Abs, it is reasonable to expect that most patients will show clinical improvement with IgG-targeting therapies. Nevertheless, future studies are needed to evaluate the long-term efficacy of such interventions and clarify the extent to which they will benefit patients harboring MuSK IgA Abs.

Additionally, in our cohort, two patients with MuSK IgA Abs were treated with RTX and followed longitudinally for several years. One patient (MuSK-2) exhibited a transient MuSK IgA response and — following two RTX cycles — achieved complete stable remission, which persisted at the last follow-up, eight years after immunosuppression withdrawal. In contrast, the other patient

(MuSK-1) experienced a protracted disease course, characterized by durable MuSK IgA positivity, clonally expanded MuSK IgA B cells, and recurrent relapses requiring chronic RTX administration. These observations suggest that sustained MuSK IgA responses may define a subset of patients who remain dependent on long-term B-cell depletion. Collectively, our findings generate new hypotheses regarding mechanisms of clinical relapse, resistance to treatment, and disease perpetuation, warranting future research.

Limitations of the study

Immunosuppressive treatments during sampling may have affected Ab levels, potentially leading to an underestimation of the true prevalence of MuSK IgA Abs. Second, given the total number of patients in our cohorts and the limited number of MuSK IgA seropositive cases, our results may not be broadly representative of the whole MuSK MG population. For several patients, however, serially collected samples were available, which allowed longitudinal tracking of their MuSK Ab levels. Third, the epitope mapping strategy employed to evaluate polyclonality may have overlooked unique clones targeting different epitopes within the same domain. In addition, while our BCR sequencing analysis identified IgA clonal variants, no evidence of MuSK IgA-IgG class-switch events was found, possibly due to limited sampling of the circulating B-cell repertoire.

Conclusions

By combining serologic profiling, generation of patient-derived mAbs, and in vitro and in vivo experiments, we characterized a novel Ab isotype in MuSK MG that offered provocative insights into disease mechanisms. Our findings provide pathways for further research investigating the role of IgA in MuSK autoimmunity and in other IgG4-driven autoimmune conditions.

Data availability

Anonymized data will be shared at request by qualified investigators following the execution of appropriate materials transfer agreements.

Acknowledgements

We thank Drs. Sarah Totten and Diana Li for providing the fab-arm exchanged MuSK1A-KLH mAb.

Funding

Dr. Gianvito Masi is supported by a Development Grant from the Muscular Dystrophy Association (MDA), a High Impact Pilot Project Award from the Myasthenia Gravis Foundation of America (MGFA), and a Shark Tank Award from the Neuromuscular Study Group (NMSG). Dr. Kenneth Hoehn is supported by National Institute of Allergy and Infectious Diseases of the NIH under award number R00AI159302. Dr. Alexandra C. Bayer is supported, in part, through an MGNet Scholar award provided by the Rare Diseases Clinical Research Consortia of the NIH and MGNet, under award number U54-NS115054. Dr. Richard J. Nowak is supported by the National Institutes of Health funded Rare Diseases Clinical Research Network (NIH-RDCRN) under award number U54NS115054 (MGNet). Dr. Kevin C. O'Connor is supported by the National Institute of Allergy and Infectious Diseases of the NIH under award numbers R01-AI114780 and through an award provided through the Rare Diseases Clinical Research Consortia of the NIH and MGNet (award number U54-NS115054). This work was also in part supported by the Else Kröner Fresenius Prize for Medical Research and the Howard Hughes Medical Institute Emerging Pathogens Initiative.

Competing interests

Dr. Masi has received a speaking honorarium from Amgen. Dr. Evoli has served as a member of the scientific award jury for Grifols, as a speaker for UCB, and as an advisory board attendant for

UCB. Dr. Hoehn receives consulting fees from Prellis Biologics. Dr. Iwasaki co-founded RIGImmune, Xanadu Bio and PanV and is a member of the Board of Directors of Roche Holding Ltd and Genentech. Dr. Nowak has received research support from the National Institutes of Health, Genentech, Inc., Alexion Pharmaceuticals, Inc., argenx, Annexon Biosciences, Inc., Ra Pharmaceuticals, Inc. (now UCB S.A.), the Myasthenia Gravis Foundation of America, Inc., Momenta Pharmaceuticals, Inc. (now Janssen), Immunovant, Inc., Grifols, S.A., and Viela Bio, Inc. (Horizon Therapeutics, now Amgen Inc.). Dr. Nowak has served as a consultant and advisor for Alexion Pharmaceuticals, Inc., argenx, Cabaletta Bio, Inc., Cour Pharmaceuticals, Ra Pharmaceuticals, Inc. (now UCB S.A.), Immunovant, Inc., Momenta Pharmaceuticals, Inc. (now Janssen), and Viela Bio, Inc. (Horizon Therapeutics, now Amgen Inc.). Dr. Kevin C. O'Connor is an equity shareholder of Cabaletta Bio; serves on advisory boards for Roche, Merck (EMD Serono), and Neurocrine Biosciences; and has received research support from Viela Bio, (now Horizon Therapeutics/Amgen), argenx, and Seismic Therapeutic.

No other disclosures were reported.

Supplementary material

Supplementary material is available at *Brain* online.

References

1. Gilhus NE. Myasthenia Gravis. *N Engl J Med*. Dec 29 2016;375(26):2570-2581. doi:10.1056/NEJMra1602678

2. Punga AR, Maddison P, Heckmann JM, Guptill JT, Evoli A. Epidemiology, diagnostics, and biomarkers of autoimmune neuromuscular junction disorders. *Lancet Neurol*. Feb 2022;21(2):176-188. doi:10.1016/S1474-4422(21)00297-0

3. Hoch W, McConville J, Helms S, Newsom-Davis J, Melms A, Vincent A. Auto-antibodies to the receptor tyrosine kinase MuSK in patients with myasthenia gravis without acetylcholine receptor antibodies. *Nat Med*. Mar 2001;7(3):365-8. doi:10.1038/85520

4. Anil R, Kumar A, Alaparthi S, et al. Exploring outcomes and characteristics of myasthenia gravis: Rationale, aims and design of registry - The EXPLORE-MG registry. *J Neurol Sci*. Jul 15 2020;414:116830. doi:10.1016/j.jns.2020.116830

5. Evoli A, Tonali PA, Padua L, et al. Clinical correlates with anti-MuSK antibodies in generalized seronegative myasthenia gravis. *Brain*. Oct 2003;126(Pt 10):2304-11. doi:10.1093/brain/awg223

6. Masi G, O'Connor KC. Novel pathophysiological insights in autoimmune myasthenia gravis. *Curr Opin Neurol*. Oct 1 2022;35(5):586-596. doi:10.1097/WCO.0000000000001088

7. Illa I, Diaz-Manera J, Rojas-Garcia R, et al. Sustained response to Rituximab in anti-AChR and anti-MuSK positive Myasthenia Gravis patients. *J Neuroimmunol*. Sep 15 2008;201-202:90-4. doi:10.1016/j.jneuroim.2008.04.039

8. Diaz-Manera J, Martinez-Hernandez E, Querol L, et al. Long-lasting treatment effect of rituximab in MuSK myasthenia. *Neurology*. Jan 17 2012;78(3):189-93. doi:10.1212/WNL.0b013e3182407982

9. Keung B, Robeson KR, DiCapua DB, et al. Long-term benefit of rituximab in MuSK autoantibody myasthenia gravis patients. *J Neurol Neurosurg Psychiatry*. Dec 2013;84(12):1407-9. doi:10.1136/jnnp-2012-303664

10. Hehir MK, Hobson-Webb LD, Benatar M, et al. Rituximab as treatment for anti-MuSK myasthenia gravis: Multicenter blinded prospective review. *Neurology*. Sep 5 2017;89(10):1069-1077. doi:10.1212/WNL.0000000000004341

11. Marino M, Basile U, Spagni G, et al. Long-Lasting Rituximab-Induced Reduction of Specific-But Not Total-IgG4 in MuSK-Positive Myasthenia Gravis. *Front Immunol*. 2020;11:613. doi:10.3389/fimmu.2020.00613

12. Spagni G, Vincent A, Sun B, et al. Serological Markers of Clinical Improvement in MuSK Myasthenia Gravis. *Neurol Neuroimmunol Neuroinflamm*. Nov 2024;11(6):e200313. doi:10.1212/NXI.0000000000200313

13. McConville J, Farrugia ME, Beeson D, et al. Detection and characterization of MuSK antibodies in seronegative myasthenia gravis. *Ann Neurol*. Apr 2004;55(4):580-4. doi:10.1002/ana.20061

14. Rispens T, Huijbers MG. The unique properties of IgG4 and its roles in health and disease. *Nat Rev Immunol*. Nov 2023;23(11):763-778. doi:10.1038/s41577-023-00871-z

15. Khani-Habibabadi F, Roy B, Pham MC, et al. AChR Autoantibody Pathogenic Properties Are Heterogeneously Distributed and Undergo Temporal Changes Among Patients With Myasthenia Gravis. *Neurol Neuroimmunol Neuroinflamm*. Sep 2025;12(5):e200436. doi:10.1212/NXI.0000000000200436

16. van der Neut Kolfschoten M, Schuurman J, Losen M, et al. Anti-inflammatory activity of human IgG4 antibodies by dynamic Fab arm exchange. *Science*. Sep 14 2007;317(5844):1554-7. doi:10.1126/science.1144603

17. Koneczny I, Stevens JA, De Rosa A, et al. IgG4 autoantibodies against muscle-specific kinase undergo Fab-arm exchange in myasthenia gravis patients. *J Autoimmun*. Feb 2017;77:104-115. doi:10.1016/j.jaut.2016.11.005

18. Klooster R, Plomp JJ, Huijbers MG, et al. Muscle-specific kinase myasthenia gravis IgG4 autoantibodies cause severe neuromuscular junction dysfunction in mice. Research Support, Non-U.S. Gov't. *Brain*. Apr 2012;135(Pt 4):1081-101. doi:10.1093/brain/aws025

19. Huijbers MG, Zhang W, Klooster R, et al. MuSK IgG4 autoantibodies cause myasthenia gravis by inhibiting binding between MuSK and Lrp4. *Proc Natl Acad Sci U S A*. Dec 17 2013;110(51):20783-8. doi:10.1073/pnas.1313944110

20. Takata K, Stathopoulos P, Cao M, et al. Characterization of pathogenic monoclonal autoantibodies derived from muscle-specific kinase myasthenia gravis patients. *JCI Insight*. Jun 20 2019;4(12):e127167. doi:10.1172/jci.insight.127167

21. Huijbers MG, Vergoossen DL, Fillie-Grijpma YE, et al. MuSK myasthenia gravis monoclonal antibodies: Valency dictates pathogenicity. *Neurol Neuroimmunol Neuroinflamm*. May 2019;6(3):e547. doi:10.1212/NXI.0000000000000547

22. Glass DJ, Bowen DC, Stitt TN, et al. Agrin acts via a MuSK receptor complex. *Cell*. May 17 1996;85(4):513-23. doi:10.1016/s0092-8674(00)81252-0

23. Xie T, Xu G, Liu Y, Quade B, Lin W, Bai XC. Structural insights into the assembly of the agrin/LRP4/MuSK signaling complex. *Proc Natl Acad Sci U S A*. Jun 6 2023;120(23):e2300453120. doi:10.1073/pnas.2300453120

24. Herbst R, Huijbers MG, Oury J, Burden SJ. Building, Breaking, and Repairing Neuromuscular Synapses. *Cold Spring Harb Perspect Biol*. May 2 2024;16(5)doi:10.1101/cshperspect.a041490

25. Koneczny I, Cossins J, Waters P, Beeson D, Vincent A. MuSK myasthenia gravis IgG4 disrupts the interaction of LRP4 with MuSK but both IgG4 and IgG1-3 can disperse preformed agrin-independent AChR clusters. *PLoS One*. 2013;8(11):e80695. doi:10.1371/journal.pone.0080695

26. Budayeva HG, Sengupta-Ghosh A, Phu L, Moffat JG, Ayalon G, Kirkpatrick DS. Phosphoproteome Profiling of the Receptor Tyrosine Kinase MuSK Identifies Tyrosine Phosphorylation of Rab GTPases. *Mol Cell Proteomics*. Apr 2022;21(4):100221. doi:10.1016/j.mcpro.2022.100221

27. Lim JL, Augustinus R, Plomp JJ, et al. Development and characterization of agonistic antibodies targeting the Ig-like 1 domain of MuSK. *Sci Rep*. May 8 2023;13(1):7478. doi:10.1038/s41598-023-32641-1

28. Vergoossen DLE, Plomp JJ, Gstottner C, et al. Functional monovalency amplifies the pathogenicity of anti-MuSK IgG4 in myasthenia gravis. *Proc Natl Acad Sci U S A*. Mar 30 2021;118(13)doi:10.1073/pnas.2020635118

29. Cao M, Liu WW, Maxwell S, et al. IgG1-3 MuSK Antibodies Inhibit AChR Cluster Formation, Restored by SHP2 Inhibitor, Despite Normal MuSK, DOK7, or AChR Subunit Phosphorylation. *Neurol Neuroimmunol Neuroinflamm*. Nov 2023;10(6)doi:10.1212/NXI.0000000000200147

30. Nihei Y, Haniuda K, Higashiyama M, et al. Identification of IgA autoantibodies targeting mesangial cells redefines the pathogenesis of IgA nephropathy. *Sci Adv*. Mar 22 2023;9(12):eadd6734. doi:10.1126/sciadv.add6734

31. Waterman HR, Dufort MJ, Posso SE, et al. Lupus IgA1 autoantibodies synergize with IgG to enhance plasmacytoid dendritic cell responses to RNA-containing immune complexes. *Sci Transl Med*. Jul 3 2024;16(754):eadl3848. doi:10.1126/scitranslmed.adl3848

32. Volkov M, Coppola M, Huizinga R, et al. Comprehensive overview of autoantibody isotype and subclass distribution. *J Allergy Clin Immunol*. Nov 2022;150(5):999-1010. doi:10.1016/j.jaci.2022.05.023

33. Bartoccioni E, Scuderi F, Minicuci GM, Marino M, Ciaraffa F, Evoli A. Anti-MuSK antibodies: correlation with myasthenia gravis severity. *Neurology*. Aug 8 2006;67(3):505-7. doi:10.1212/01.wnl.0000228225.23349.5d

34. Niks EH, van Leeuwen Y, Leite MI, et al. Clinical fluctuations in MuSK myasthenia gravis are related to antigen-specific IgG4 instead of IgG1. *J Neuroimmunol*. Mar 2008;195(1-2):151-6. doi:10.1016/j.jneuroim.2008.01.013

35. Fichtner ML, Hoehn KB, Ford EE, et al. Reemergence of pathogenic, autoantibody-producing B cell clones in myasthenia gravis following B cell depletion therapy. *Acta Neuropathol Commun*. Oct 28 2022;10(1):154. doi:10.1186/s40478-022-01454-0

36. Pham MC, Masi G, Patzina R, et al. Individual myasthenia gravis autoantibody clones can efficiently mediate multiple mechanisms of pathology. *Acta Neuropathol*. Aug 2023;146(2):319-336. doi:10.1007/s00401-023-02603-y

37. Stathopoulos P, Kumar A, Nowak RJ, O'Connor KC. Autoantibody-producing plasmablasts after B cell depletion identified in muscle-specific kinase myasthenia gravis. *JCI Insight*. Sep 07 2017;2(17):e94263-e94275. doi:10.1172/jci.insight.94263

38. Woof JM, Russell MW. Structure and function relationships in IgA. *Mucosal Immunol*. Nov 2011;4(6):590-7. doi:10.1038/mi.2011.39

39. Fichtner ML, Vieni C, Redler RL, et al. Affinity maturation is required for pathogenic monovalent IgG4 autoantibody development in myasthenia gravis. *J Exp Med*. Dec 7 2020;217(12):e20200513. doi:10.1084/jem.20200513

40. Mandel-Brehm C, Fichtner ML, Jiang R, et al. Elevated N-Linked Glycosylation of IgG V Regions in Myasthenia Gravis Disease Subtypes. *J Immunol*. Oct 15 2021;207(8):2005-2014. doi:10.4049/jimmunol.2100225

41. Koers J, Sciarrillo R, Derksen NIL, et al. Differences in IgG autoantibody Fab glycosylation across autoimmune diseases. *J Allergy Clin Immunol*. Jun 2023;151(6):1646-1654. doi:10.1016/j.jaci.2022.10.035

42. Till JH, Becerra M, Watty A, et al. Crystal structure of the MuSK tyrosine kinase: insights into receptor autoregulation. *Structure*. Sep 2002;10(9):1187-96. doi:10.1016/s0969-2126(02)00814-6

43. Stiegler AL, Burden SJ, Hubbard SR. Crystal structure of the agrin-responsive immunoglobulin-like domains 1 and 2 of the receptor tyrosine kinase MuSK. *J Mol Biol*. Dec 1 2006;364(3):424-33. doi:10.1016/j.jmb.2006.09.019

44. Stiegler AL, Burden SJ, Hubbard SR. Crystal structure of the frizzled-like cysteine-rich domain of the receptor tyrosine kinase MuSK. *J Mol Biol*. Oct 16 2009;393(1):1-9. doi:10.1016/j.jmb.2009.07.091

45. Huijbers MG, Vink AF, Niks EH, et al. Longitudinal epitope mapping in MuSK myasthenia gravis: implications for disease severity. *J Neuroimmunol*. Feb 15 2016;291:82-8. doi:10.1016/j.jneuroim.2015.12.016

46. Hoehn KB, Turner JS, Miller FI, et al. Human B cell lineages associated with germinal centers following influenza vaccination are measurably evolving. *Elife*. Nov 17 2021;10doi:10.7554/eLife.70873

47. Linnington C, Webb M, Woodhams PL. A novel myelin-associated glycoprotein defined by a mouse monoclonal antibody. *J Neuroimmunol*. Sep-Oct 1984;6(6):387-96. doi:10.1016/0165-5728(84)90064-x

48. Labrijn AF, Meesters JI, Priem P, et al. Controlled Fab-arm exchange for the generation of stable bispecific IgG1. *Nat Protoc*. Oct 2014;9(10):2450-63. doi:10.1038/nprot.2014.169

49. Morsch M, Reddel SW, Ghazanfari N, Toyka KV, Phillips WD. Muscle specific kinase autoantibodies cause synaptic failure through progressive wastage of postsynaptic acetylcholine receptors. *Exp Neurol*. Oct 2012;237(2):286-95. doi:10.1016/j.expneurol.2012.06.034

50. Boross P, Lohse S, Nederend M, et al. IgA EGFR antibodies mediate tumour killing in vivo. *EMBO Mol Med*. Aug 2013;5(8):1213-26. doi:10.1002/emmm.201201929

51. Desestret V, Chefdeville A, Viaccoz A, et al. CSF IgA NMDAR antibodies are potential biomarkers for teratomas in anti-NMDAR encephalitis. *Neurol Neuroimmunol Neuroinflamm*. Dec 2015;2(6):e166. doi:10.1212/NXI.0000000000000166

52. Pruss H, Holtje M, Maier N, et al. IgA NMDA receptor antibodies are markers of synaptic immunity in slow cognitive impairment. *Neurology*. May 29 2012;78(22):1743-53. doi:10.1212/WNL.0b013e318258300d

53. Ayroza Galvao Ribeiro Gomes AB, Kulsvehagen L, Lipps P, et al. Immunoglobulin A Antibodies Against Myelin Oligodendrocyte Glycoprotein in a Subgroup of Patients With Central Nervous System Demyelination. *JAMA Neurol*. Sep 1 2023;80(9):989-995. doi:10.1001/jamaneurol.2023.2523

54. Young C, Singh M, Jackson KJL, et al. A triad of somatic mutagenesis converges in self-reactive B cells to cause a virus-induced autoimmune disease. *Immunity*. Feb 11 2025;58(2):412-430 e10. doi:10.1016/j.immuni.2024.12.011

55. Dighiero G, Lymberi P, Holmberg D, Lundquist I, Coutinho A, Avrameas S. High frequency of natural autoantibodies in normal newborn mice. *J Immunol*. Feb 1985;134(2):765-71.

56. Coutinho A, Kazatchkine MD, Avrameas S. Natural autoantibodies. *Curr Opin Immunol*. Dec 1995;7(6):812-8. doi:10.1016/0952-7915(95)80053-0

57. Bunker JJ, Erickson SA, Flynn TM, et al. Natural polyreactive IgA antibodies coat the intestinal microbiota. *Science*. Oct 20 2017;358(6361)doi:10.1126/science.aan6619

58. Cerutti A. The regulation of IgA class switching. *Nat Rev Immunol*. Jun 2008;8(6):421-34. doi:10.1038/nri2322

59. Pabst O, Slack E. IgA and the intestinal microbiota: the importance of being specific. *Mucosal Immunol*. Jan 2020;13(1):12-21. doi:10.1038/s41385-019-0227-4

60. van Egmond M, van Garderen E, van Spriel AB, et al. FcalphaRI-positive liver Kupffer cells: reappraisal of the function of immunoglobulin A in immunity. *Nat Med*. Jun 2000;6(6):680-5. doi:10.1038/76261

61. Pereira MS, Kriegel MA. Evolving concepts of host-pathobiont interactions in autoimmunity. *Curr Opin Immunol*. Feb 2023;80:102265. doi:10.1016/j.coi.2022.102265

62. Chriswell ME, Lefferts AR, Clay MR, et al. Clonal IgA and IgG autoantibodies from individuals at risk for rheumatoid arthritis identify an arthritogenic strain of Subdoligranulum. *Sci Transl Med*. Oct 26 2022;14(668):eabn5166. doi:10.1126/scitranslmed.abn5166

63. Brewer RC, Lanz TV, Hale CR, et al. Oral mucosal breaks trigger anti-citrullinated bacterial and human protein antibody responses in rheumatoid arthritis. *Sci Transl Med*. Feb 22 2023;15(684):eabq8476. doi:10.1126/scitranslmed.abq8476

64. Oury J, Gamallo-Lana B, Santana L, et al. Agonist antibody to MuSK protects mice from MuSK myasthenia gravis. *Proc Natl Acad Sci U S A*. Sep 24 2024;121(39):e2408324121. doi:10.1073/pnas.2408324121

65. Halliez M, Cottin S, You A, et al. MuSK cysteine-rich domain antibodies are pathogenic in a mouse model of autoimmune myasthenia gravis. *J Clin Invest*. Aug 1 2025;135(15)doi:10.1172/JCI173308

66. Glass DJ, Apel ED, Shah S, et al. Kinase domain of the muscle-specific receptor tyrosine kinase (MuSK) is sufficient for phosphorylation but not clustering of acetylcholine receptors: required role for the MuSK ectodomain? *Proc Natl Acad Sci U S A*. Aug 5 1997;94(16):8848-53. doi:10.1073/pnas.94.16.8848

67. Zhou H, Glass DJ, Yancopoulos GD, Sanes JR. Distinct domains of MuSK mediate its abilities to induce and to associate with postsynaptic specializations. *J Cell Biol*. Sep 6 1999;146(5):1133-46. doi:10.1083/jcb.146.5.1133

68. Rose N, Holdermann S, Callegari I, et al. Receptor clustering and pathogenic complement activation in myasthenia gravis depend on synergy between antibodies with multiple subunit specificities. *Acta Neuropathol*. Nov 2022;144(5):1005-1025. doi:10.1007/s00401-022-02493-6

69. Garcia A, Rodriguez S, Dugast E, et al. Durable B-Cell Impairment While Sparing IgA B Cells After Ocrelizumab Therapy in Multiple Sclerosis. *Ann Clin Transl Neurol*. Aug 8 2025;doi:10.1002/acn3.70135

70. Crickx E, Chappert P, Sokal A, et al. Rituximab-resistant splenic memory B cells and newly engaged naive B cells fuel relapses in patients with immune thrombocytopenia. *Sci Transl Med*. Apr 14 2021;13(589)doi:10.1126/scitranslmed.abc3961

71. Tur C, Eckstein M, Velden J, et al. CD19-CAR T-cell therapy induces deep tissue depletion of B cells. *Ann Rheum Dis*. Sep 11 2024;doi:10.1136/ard-2024-226142

72. Mei HE, Frolich D, Giesecke C, et al. Steady-state generation of mucosal IgA+ plasmablasts is not abrogated by B-cell depletion therapy with rituximab. *Blood*. Dec 9 2010;116(24):5181-90. doi:10.1182/blood-2010-01-266536

73. Ellebrecht CT, Mukherjee EM, Zheng Q, et al. Autoreactive IgG and IgA B Cells Evolve through Distinct Subclass Switch Pathways in the Autoimmune Disease Pemphigus Vulgaris. *Cell Rep*. Aug 28 2018;24(9):2370-2380. doi:10.1016/j.celrep.2018.07.093

74. Howard JF, Jr., Bril V, Vu T, et al. Safety, efficacy, and tolerability of efgartigimod in patients with generalised myasthenia gravis (ADAPT): a multicentre, randomised, placebo-controlled, phase 3 trial. *Lancet Neurol*. Jul 2021;20(7):526-536. doi:10.1016/S1474-4422(21)00159-9

75. Bril V, Druzdz A, Grosskreutz J, et al. Safety and efficacy of rozanolixizumab in patients with generalised myasthenia gravis (MycarinG): a randomised, double-blind, placebo-controlled, adaptive phase 3 study. *Lancet Neurol*. May 2023;22(5):383-394. doi:10.1016/S1474-4422(23)00077-7

76. Sudol ASL, Butler J, Ivory DP, Tews I, Crispin M. Extensive substrate recognition by the streptococcal antibody-degrading enzymes IdeS and EndoS. *Nat Commun*. Dec 17 2022;13(1):7801. doi:10.1038/s41467-022-35340-z

Figure legends

Figure 1 MuSK-specific IgA Abs are detected in a subset of patients with MuSK MG. (A) Validation of the specificity of a commercial anti-IgA secondary antibody using MuSK1B, a MuSK-specific human mAb subcloned into an IgG1, IgG2, IgG3, IgG4, IgA1 and IgM backbone. Binding of isotype- and subclass-specific monoclonal antibodies (mAbs) was detected using flow cytometry. **(B)** MuSK IgA screening of 112 MuSK MG, 30 HD and 32 AChR MG sera (discovery cohort). The cutoff for positivity (dashed line) was set at the median MFI ratio of the HD group + four standard deviations (SDs). Each data point represents the mean of experimental duplicates.

CBA-positive sera are color-coded, with each color corresponding to a distinct patient. **(C)** MuSK IgA screening of a validation cohort including 23 MuSK MG and 25 HD sera. (**D)** Cell-based assays using confocal fluorescence microscopy. Representative images include a healthy donor (HD) and three MuSK MG patients, two of whom (MuSK-1 and MuSK-4), belonging to independent cohorts, tested positive for both MuSK IgG and IgA Abs, while MuSK-5 only harbored MuSK IgG Abs. First row: nuclei counterstained with DAPI. Second row: eGFP signal showing MuSK-expressing cells. Third row: IgG (cyan) and IgA (red) detection is shown for each representative case. Fourth row: merge, confirming co-localization of IgG and/or IgA (when detected) with MuSK-expressing cells. All images were captured at 63× magnification. Scale bar: 20μm. **(E)** Correlation between MuSK IgA and MuSK IgG antibody levels, assessed using Pearson correlation coefficient. **(F)** Longitudinal tracking of serum MuSK IgG and IgA levels in a patient (MuSK-1) with fourteen serum samples (timepoints) collected over a decade of disease activity. Full circles represent serum samples above the positivity cutoff, while empty circles indicate those below the cutoff. **(G)** Panels showing superimposed changes of MuSK IgG and IgA levels between two timepoints. The upper panel corresponds to timepoints 11-12 (months 69-78), while the lower panel corresponds to timepoints 13-14 (months 127-138).

Figure 2 Binding properties of patient-derived MuSK-specific IgA mAbs. (A) Binding curves of three MuSK-specific IgA mAbs tested in a MuSK cell-based assay over a range of serial dilutions. MuSK1B (specific to MuSK) and mAb01a (specific to AChR), both expressed as IgA isotype antibodies, were used as experimental controls. The y-axis shows the calculated MFI ratio of the anti-IgA secondary antibody, representing binding of the mAbs to MuSK. All data are presented as a mean of experimental triplicates and SDs. **(B)** Cell-based assays using confocal fluorescence microscopy, confirming the specificity of the IgA mAbs. First row: nuclei counterstained with DAPI. Second row: eGFP signal showing MuSK-expressing cells. Third row: anti-IgA secondary antibody signal. Fourth row (merge): for aMu1, aMu2, aMu3 and MuSK1B, the IgA binding signal (red fluorescence on cell membrane) colocalizes with MuSK-expressing cells (green fluorescence), indicating MuSK recognition of individual mAbs. All images were captured at 63X magnification. Scale bar: 20μm. **(C)** Bar graph displaying the domain mapping results. All mAbs were subcloned into IgG1 vectors and tested for binding to HEK293T cells

expressing different MuSK domains. MuSK mAbs binding to three different MuSK domains were used as controls. A negative control mAb (mAb09) was also included. The y-axis represents the MFI ratio of an anti-IgG-AF647 antibody. Experimental triplicates were run for each test. The means of triplicate values and SDs are shown. **(D)** Heatmap showing binding competition between MuSK-specific IgA and IgG4 mAbs. The x-axis shows three IgG4 mAbs (tested in a bivalent format), while the y-axis lists three MuSK-specific IgA mAbs and mAb01a-IgA (AChR-specific), used as a control. For each pairing, IgG binding (expressed as MFI ratio) was normalized to the non-competing condition. The color intensity correlates with the competition level shown by each IgA-IgG4 combination. Black represents the highest level of competition. **(E)** Schematic of the MuSK extracellular domain and the binding specificities of the IgA and IgG4 mAbs included in the study (mAbs with the same color compete for identical or partially overlapping epitopes).

Figure 3 Longitudinal durability of a clonally expanded MuSK-specific IgA clone. (A) Clonal variants (CVs) of the MuSK-specific mAb aMu1 were identified in longitudinally collected samples from patient MuSK-1. The graph shows the identification of 24 distinct CVs (indicated by arrows) spanning 77 months of disease activity. The detection of MuSK IgA in serum (red circles) is also shown. **(B)** Clonal lineage tree containing BCR sequences from bulk RNA sequencing of serial samples from patient MuSK-1 from whom aMu1 was cloned. A maximum likelihood tree of aMu1 is shown, with 24 IgA CVs. Edge lengths represent the expected number of intervening somatic mutations between nodes (see scale bar). Colors correspond to the collection time point (months) at which each sequence was identified in relation to the first available collection timepoint. Duplicate sequences or those differing only by ambiguous nucleotides were collapsed, as indicated by the size of each tip. (**C**) Schematic diagram illustrating five representative clonal variants (CV1-5) of aMu1. Lollipop-shaped symbols indicate nonsynonymous nucleotide mutations as compared with the germline IGHV4-34 gene. Amino acid replacement residues are indicated under each symbol. The amino acids replaced in the germline gene segment (IGHV4-34) from which aMu1 derived are indicated in red. Right: heatmap summarizing the cell-based assay results that confirmed MuSK specificity for the five representative CVs. An AChR-specific mAb (mAb01a), subcloned into an IgA1 vector, was used as a negative control.

Figure 4 Individual IgA mAbs demonstrate a dual role, acting both as MuSK agonists and as antagonists to pathogenic monovalent IgG4 autoantibodies. The addition of neural agrin to C2C12 myotubes leads to activation of MuSK and the formation of AChR clusters that can be readily visualized with fluorescent α-bungarotoxin and then quantified. **(A)** Assessment of the agonistic capacity of three MuSK IgA mAbs (aMu1 aMu2 and aMu3) in the absence of agrin. 8-18C5, a mAb that binds to MOG, was subcloned into an IgA1 backbone and used as a control. The number of AChR clusters is normalized to the agrin-only effect of each individual experiment (red line). Each data point represents the mean value obtained from two wells (six image fields) with fully differentiated myotubes, and for each condition at least three independent experiments were performed. Bars represent the mean of means and error bars SDs. Multiple comparisons ANOVA (against 8-18C5 mAb), Dunnett's test; * $p<0.05$, ** $p<0.01$, *** $p<0.001$, **** $p<0.0001$, only shown when significant. Representative microscopy images for each condition are shown below the graph. The panels in the bottom left corner of each image show magnifications of representative areas to highlight AChR clustering (red arrow). Scale bar: 100 μm. DM: differentiation media. **(B)** Normalized densitometry analysis results from the MuSK phosphorylation immunoblots are plotted. Each data point represents an independent immunoblot experiment. Bars represent the mean and error bars SDs. Phosphorylation of MuSK (detected by a commercial anti-phosphotyrosine antibody) was normalized to MuSK expression (detected by a commercial anti-MuSK antibody after stripping the blot). The ratio of phosphorylated MuSK/total MuSK is plotted. Multiple-comparisons ANOVA (against 8-185C IgA), Dunnett's test; * $p<0.05$, ** $p<0.01$, *** $p<0.001$, **** $p<0.0001$, only shown when significant. Below the graph is a representative immunoblot showing phosphotyrosine bands and relative MuSK expression of C2C12 myotubes following incubation with differentiation media (DM), agrin, the three MuSK IgA mAbs (aMu1, aMu2, aMu3) or a mAb control (8-18C5 IgA). **(C)** The three IgA mAbs were tested as described in **(A),** but with the addition of agrin. **(D-F)** Three MuSK IgG4-derived Fabs (MuSK1A, 6C6 and 2E6) were tested on C2C12 myotubes with agrin alone or with the addition of a MuSK-specific IgA mAb at equimolar concentrations. AChR clusters were quantified as described above. Bars represent the mean of means and error bars SDs. Multiple comparisons ANOVA (against each Fab), Dunnett's test; * $p<0.05$, ** $p<0.01$, *** $p<0.001$, **** $p<0.0001$, only shown when significant.

Figure 5 MuSK IgA mAbs act synergistically when combined, resulting in enhanced pathogenicity and potent inhibition of AChR clustering. (A) Serum IgA domain-mapping demonstrating targeting of multiple MuSK domains in two patients (MuSK-2 and MuSK-4). A conservative IgA binding cutoff (>1.5) was used. **(B)** Representative microscopy images showing the effect of combined aMu1 and aMu3 on AChR cluster formation. Scale bar: 100 μm. **(C)** Quantification of clusters in the absence agrin. (**D**) Quantification of clusters in the presence of agrin. In both experiments 8-18C5, a MOG-specific mAb, was included as an additional control. 8-18C5, aMu1 and aMu3 were combined in various permutations for analysis. The number of AChR clusters was normalized to the agrin-only effect of each individual experiment (red line). Each data point represents the mean value obtained from two wells (six image fields in total) with fully differentiated myotubes, and for each condition at least three independent experiments were performed. Bars represent the mean of means and error bars SDs. Multiple comparisons ANOVA (against aMu1+aMu3), Dunnett's test; * $p<0.05$, ** $p<0.01$, *** $p<0.001$, **** $p<0.0001$, only shown when significant.

Figure 6 Passive transfer of two MuSK-specific IgA mAbs causes myasthenic symptoms in NOD-SCID mice. (A) Experimental design of passive immunization with recombinant IgA mAbs. NOD-SCID mice (n=5 per group) received a daily IP injection of either KLH IgA (control mAb) or a mixture (1:1) of two IgA MuSK mAbs (aMu1 and aMu3); final mAb concentration: 5 mg/Kg. **(B)** Body weight measurement. **(C)** Grip strength assessment. (**D**) Rolling loop and (**E**) inverted mesh hanging tests. Data represent mean and error bars SDs. Two-tailed unpaired t test. ** $p<0.01$. **(F)** Cell-based assay testing of MuSK IgA Abs in blood samples collected on day 9. **(G)** Detection of bound IgA mAbs, colocalizing with NMJs, in whole-mount preparations of epitrochleoanconeus. Top panel: alpha-bungarotoxin (green signal), labelling NMJs. Mid panel: anti-IgA signal (red signal). Bottom panel (merge): colocalization of bungarotoxin and anti-IgA signals, confirming the deposition of IgA Abs on NMJs. Scale bar: 20 μm. **(H)** Confocal microscopy images at low (20X) and high magnification (63X) showing the morphology of representative NMJs on diaphragm muscle preparations.

Figure 7 Speculative working model for MuSK IgA autoantibody-mediated pathogenic mechanisms. (A) In the healthy neuromuscular junction (NMJ), neural agrin is secreted from motor nerve terminals and binds to LRP4 on the postsynaptic membrane, enhancing MuSK-LRP4 interaction and promoting MuSK dimerization and (auto)phosphorylation of its cytoplasmic domain. Activated MuSK initiates a complex intracellular cascade that culminates in AChR clustering, which is essential for efficient neuromuscular transmission (levels of clustering are denoted as +++/++/+ throughout the whole schematic). **(B)** MuSK IgG4 Abs act through their functional monovalency (which prevents cross-linking of MuSK) and sterically block MuSK-LRP4 binding, thereby inhibiting agrin-dependent signaling. This results in a marked impairment of AChR clustering and the failure of neuromuscular transmission. Compellingly, passive transfer of MuSK1A, a patient-derived IgG4 mAb — expressed as a bispecific mAb (MuSK1A-KLH) to emulate IgG4 monovalency — induced myasthenic symptoms in passively immunized mice. **(C)** MuSK IgA Abs, unlike IgG4 Abs, are structurally bivalent and thus capable of cross-linking and activating MuSK. As single monoclonal species, they behave as MuSK agonists and promote clustering (+/++). Furthermore, it is conceivable that each Ab can interfere with agrin signaling (similar to pathogenic IgG4 Abs), thereby hampering agrin-dependent clustering activity. Due to the concurrent agonistic potency, however, the net effect of single IgA clones is only a partial reduction in clusters compared to the agrin-only effect. This reduction may lead to no or modest pathogenicity. **(D)** When multiple MuSK IgA Abs of different epitope specificities are present (e.g., in a polyclonal response), their combined bivalency can result in dysfunctional cross-linking. This multivalent binding may hamper signaling pathways associated with the MuSK ectodomain or it kinase activity, leading to impaired cluster formation. In this case, the inhibitory mechanisms of multiple IgA clones outweigh the agonism of single clones, and agrin-mediated clustering is severely diminished, resulting in conspicuous pathogenic effects. In keeping with this, co-administration of two IgA mAbs (aMu1 and aMu3) induced muscle weakness in vivo. In aggregate, this mechanistic model proposes that the pathogenic capacity of MuSK IgA and potentially of other bivalent Abs is enhanced by the synergistic action of multiple clones. Single bivalent clones may partially counteract MuSK IgG4 Abs' effect due to their agonistic potency (**E**), but multiple clones can override MuSK agonism and demonstrate cooperative pathogenicity.

Table 1. Molecular characteristics of MuSK-specific human recombinant IgA mAbs

mAb ID	Isotype and subclass	V-(D)-J genes and alleles	AA replacements in variable region gene segment	AA replacements in CDR3	N-linked glycosylation site counts
aMu1	IgA1	IGHV4-34*01, IGHJ4*02, IGHD1-7*01	24	2	2 (germline-encoded)
	Igκ	IGKV3-20*01, IGKJ1*01	17	1	0
aMu2	IgA1	IGHV1-69*09, IGHJ1*01, IGHD5-12*01	19	4	0
	Igκ	IGKV3-11*01, IGKJ2*01 (or IGKJ2*02)	12	4	0
aMu3	IgA1	IGHV3-23*04, IGHJ5*02, IGHD3-16*02	14	5	0
	Igλ	IGLV2-18*02, IGLJ1*01	11	2	0

The IMGT database top-predicted V(D)J genes, V gene and CDR3 amino acid (AA) replacements, and number of V gene N-linked glycosylation (N-Glyc) sites are shown for both heavy and light chain pairs. V gene AA mutations were counted from the first codon of framework 1 to the invariable cysteine (C) at position 104. CDR3 AA mutations were counted between cysteine 104 and the invariable tryptophan (W) or phenylalanine (F) at position 118 in the heavy and light chain respectively, considering only mutations identified through alignment to V(D)J genes and excluding untemplated nucleotides. N-linked glycosylation motif: N-X-S/T, where X is any AA except proline. AA: amino acid; CDR3: complementarity determining region 3.

Figure 1

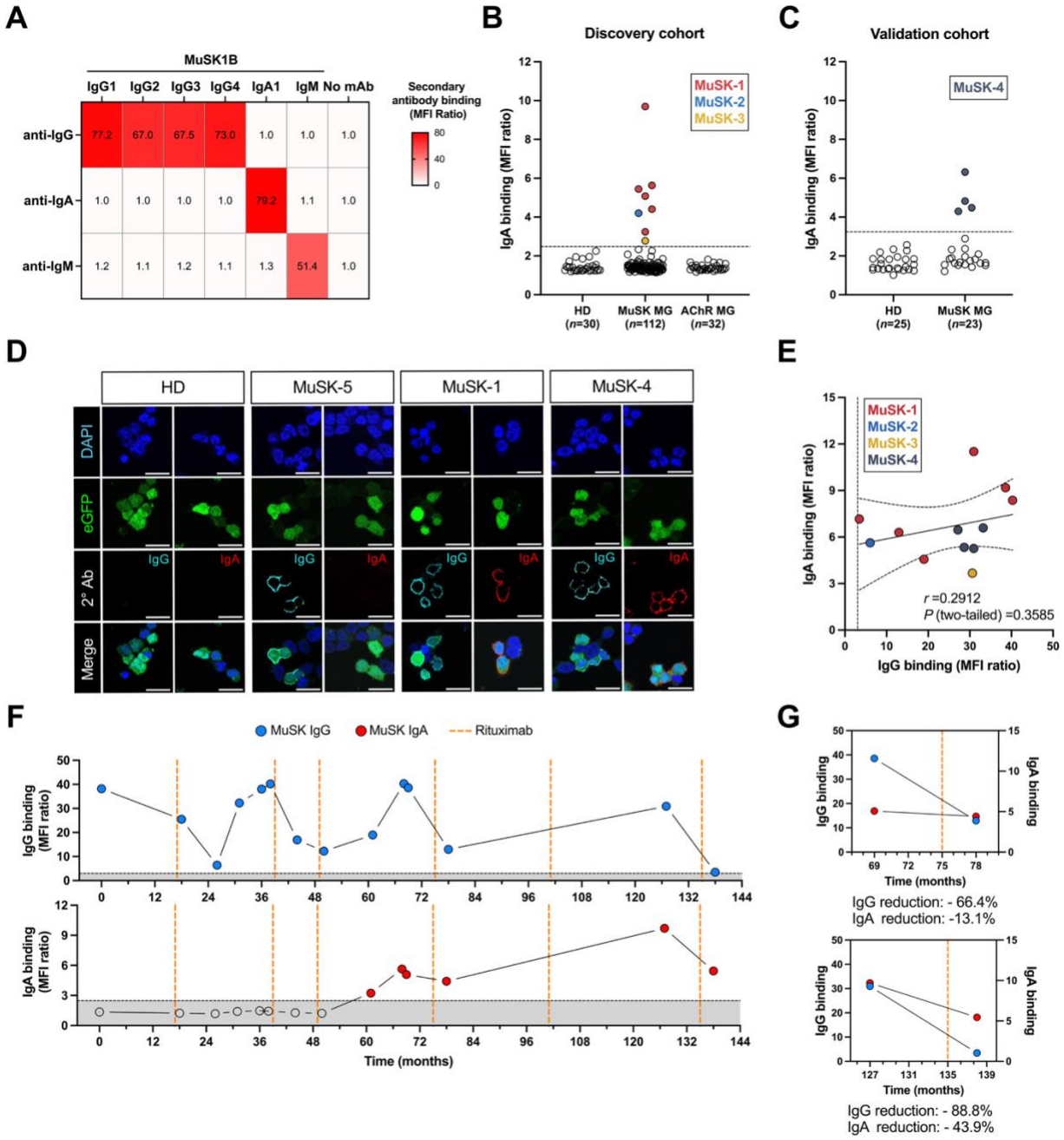
A
MuSK1B
IgG1 IgG2 IgG3 IgG4 IgA1 IgM No mAb
anti-IgG 77.2 67.0 67.5 73.0 1.0 1.0 1.0
anti-IgA 1.0 1.0 1.0 1.0 79.2 1.1 1.0
anti-IgM 1.2 1.1 1.2 1.1 1.3 51.4 1.0
Secondary antibody binding (MFI Ratio)
80
40
0
B
Discovery cohort
MuSK-1
MuSK-2
MuSK-3
IgA binding (MFI ratio)
HD (n=30)
MuSK MG (n=112)
AChR MG (n=32)
C
Validation cohort
MuSK-4
IgA binding (MFI ratio)
HD (n=25)
MuSK MG (n=23)
D
HD
MuSK-5
MuSK-1
MuSK-4
DAPI
eGFP
2° Ab
IgG
IgA
Merge
E
MuSK-1
MuSK-2
MuSK-3
MuSK-4
IgA binding (MFI ratio)
r =0.2912
P (two-tailed) =0.3585
IgG binding (MFI ratio)
F
MuSK IgG
MuSK IgA
Rituximab
IgG binding (MFI ratio)
IgA binding (MFI ratio)
Time (months)
G
IgG binding
IgA binding
Time (months)
IgG reduction: - 66.4%
IgA reduction: -13.1%
IgG reduction: - 88.8%
IgA reduction: - 43.9%

Figure 2

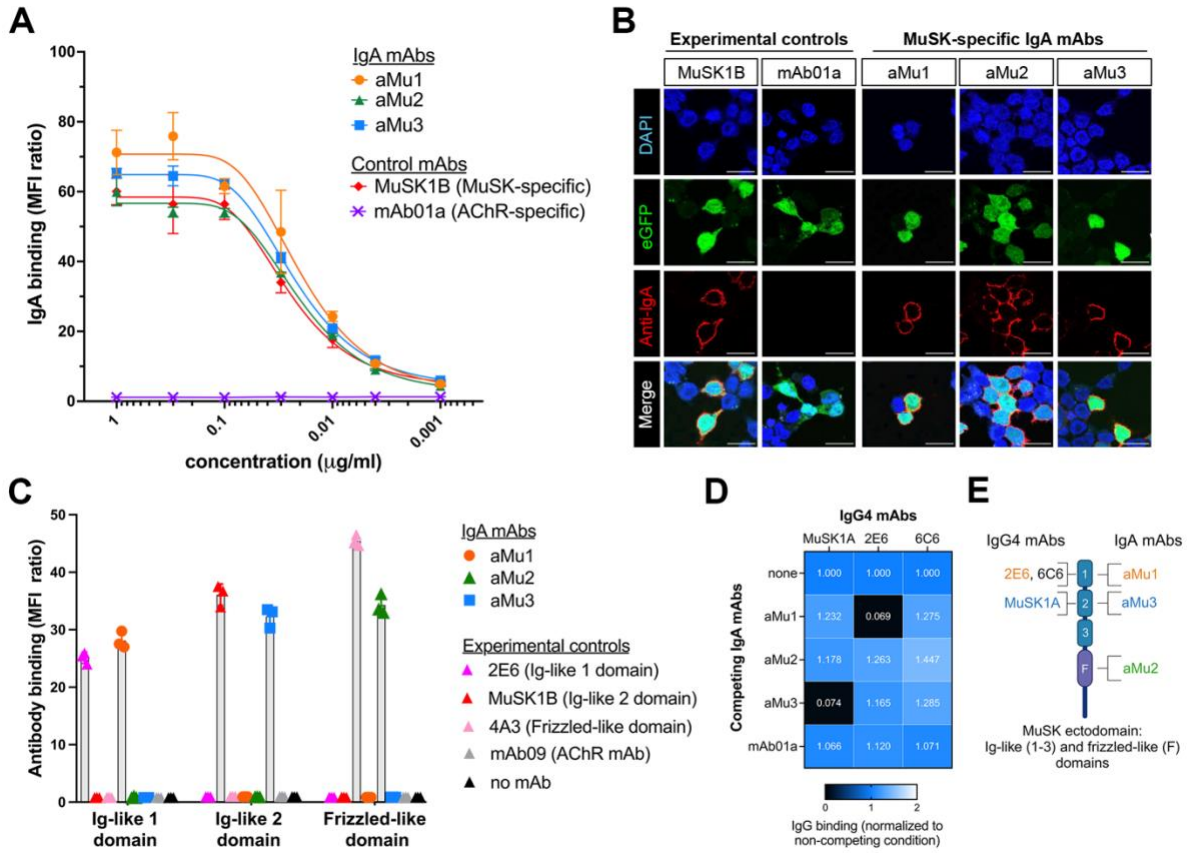
A
IgA binding (MFI ratio)
concentration (μg/ml)
IgA mAbs
aMu1
aMu2
aMu3
Control mAbs
MuSK1B (MuSK-specific)
mAb01a (AChR-specific)
B
Experimental controls
MuSK-specific IgA mAbs
MuSK1B
mAb01a
aMu1
aMu2
aMu3
DAPI
eGFP
Anti-IgA
Merge
C
Antibody binding (MFI ratio)
Ig-like 1 domain
Ig-like 2 domain
Frizzled-like domain
IgA mAbs
aMu1
aMu2
aMu3
Experimental controls
2E6 (Ig-like 1 domain)
MuSK1B (Ig-like 2 domain)
4A3 (Frizzled-like domain)
mAb09 (AChR mAb)
no mAb
D
IgG4 mAbs
MuSK1A
2E6
6C6
Competing IgA mAbs
none
aMu1
aMu2
aMu3
mAb01a
IgG binding (normalized to non-competing condition)
E
IgG4 mAbs
IgA mAbs
2E6, 6C6
MuSK1A
aMu1
aMu3
aMu2
MuSK ectodomain: Ig-like (1-3) and frizzled-like (F) domains

Figure 3

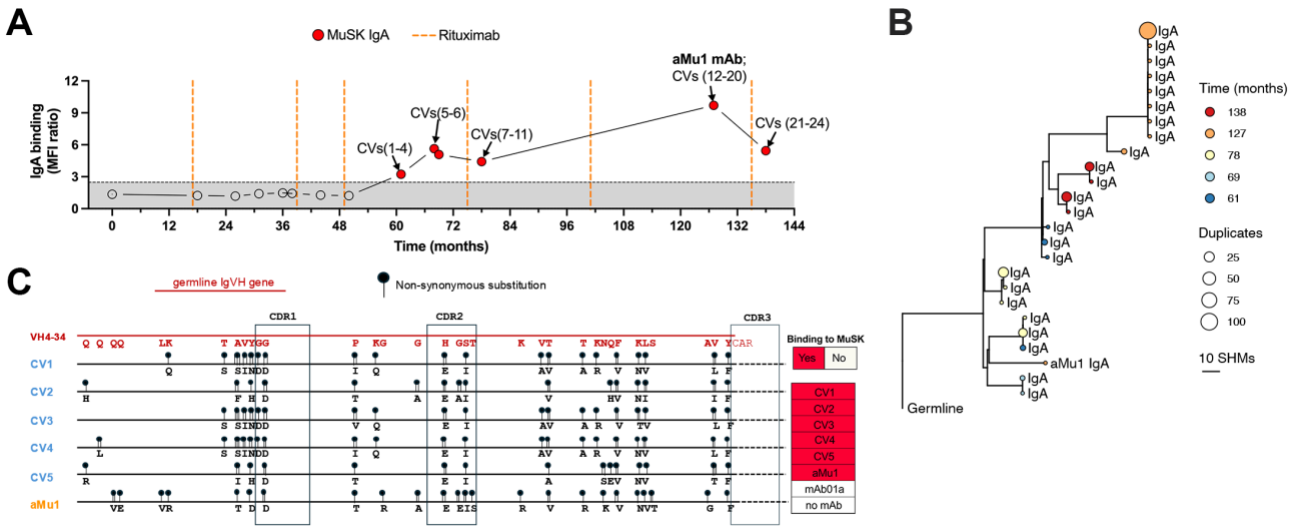
A
MuSK IgA
Rituximab
aMu1 mAb;
CVs (12-20)
CVs(5-6)
CVs(7-11)
CVs(1-4)
CVs (21-24)
IgA binding
(MFI ratio)
Time (months)
B
Time (months)
138
127
78
69
61
Duplicates
25
50
75
100
10 SHMs
aMu1 IgA
Germline
C
germline IgVH gene
Non-synonymous substitution
CDR1
CDR2
CDR3
VH4-34
CV1
CV2
CV3
CV4
CV5
aMu1
Binding to MuSK
Yes
No
mAb01a
no mAb

Figure 4

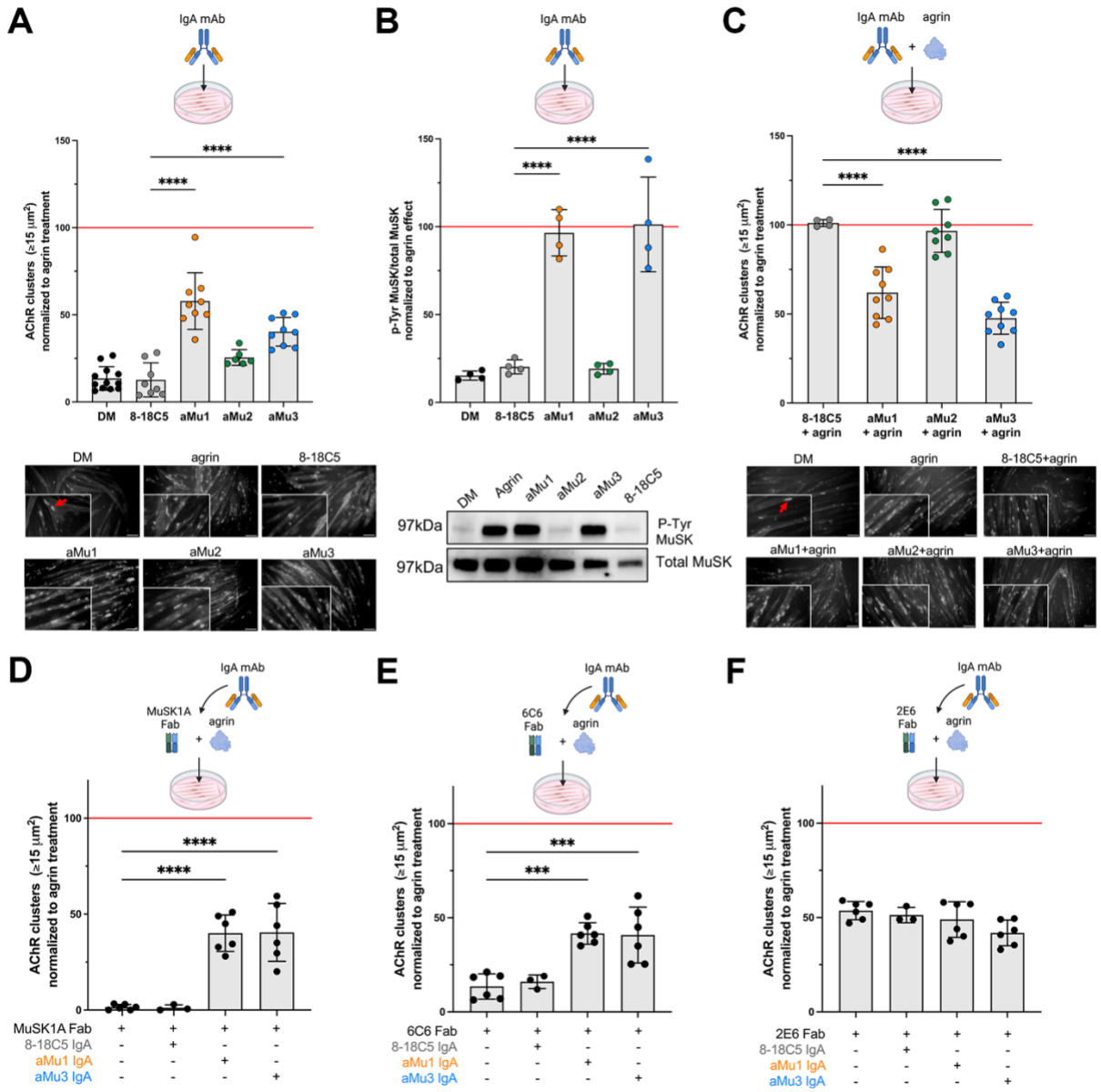
A
IgA mAb
AChR clusters (≥15 µm²) normalized to agrin treatment
DM
8-18C5
aMu1
aMu2
aMu3
B
IgA mAb
p-Tyr MuSK/total MuSK normalized to agrin effect
97kDa
P-Tyr MuSK
Total MuSK
C
IgA mAb
agrin
8-18C5 + agrin
aMu1 + agrin
aMu2 + agrin
aMu3 + agrin
8-18C5+agrin
aMu1+agrin
aMu2+agrin
aMu3+agrin
D
MuSK1A Fab
MuSK1A Fab
8-18C5 IgA
aMu1 IgA
aMu3 IgA
E
6C6 Fab
6C6 Fab
F
2E6 Fab
2E6 Fab

Figure 5

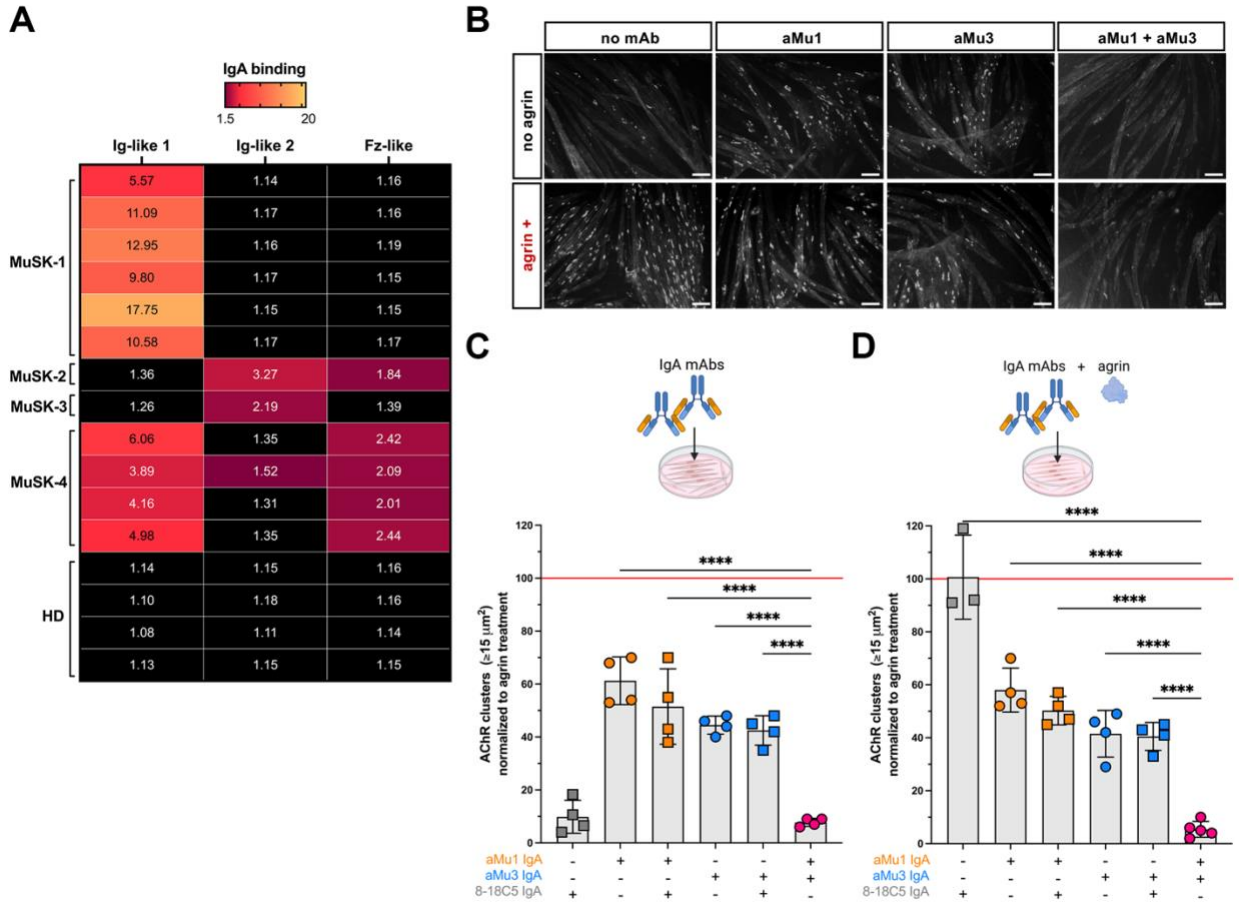
A
IgA binding
1.5
20
Ig-like 1
Ig-like 2
Fz-like
MuSK-1
MuSK-2
MuSK-3
MuSK-4
HD
5.57 1.14 1.16
11.09 1.17 1.16
12.95 1.16 1.19
9.80 1.17 1.15
17.75 1.15 1.15
10.58 1.17 1.17
1.36 3.27 1.84
1.26 2.19 1.39
6.06 1.35 2.42
3.89 1.52 2.09
4.16 1.31 2.01
4.98 1.35 2.44
1.14 1.15 1.16
1.10 1.18 1.16
1.08 1.11 1.14
1.13 1.15 1.15
B
no mAb
aMu1
aMu3
aMu1 + aMu3
no agrin
agrin +
C
IgA mAbs
AChR clusters (≥15 µm²) normalized to agrin treatment
aMu1 IgA
aMu3 IgA
8-18C5 IgA
D
IgA mAbs + agrin
AChR clusters (≥15 µm²) normalized to agrin treatment
aMu1 IgA
aMu3 IgA
8-18C5 IgA

Figure 6

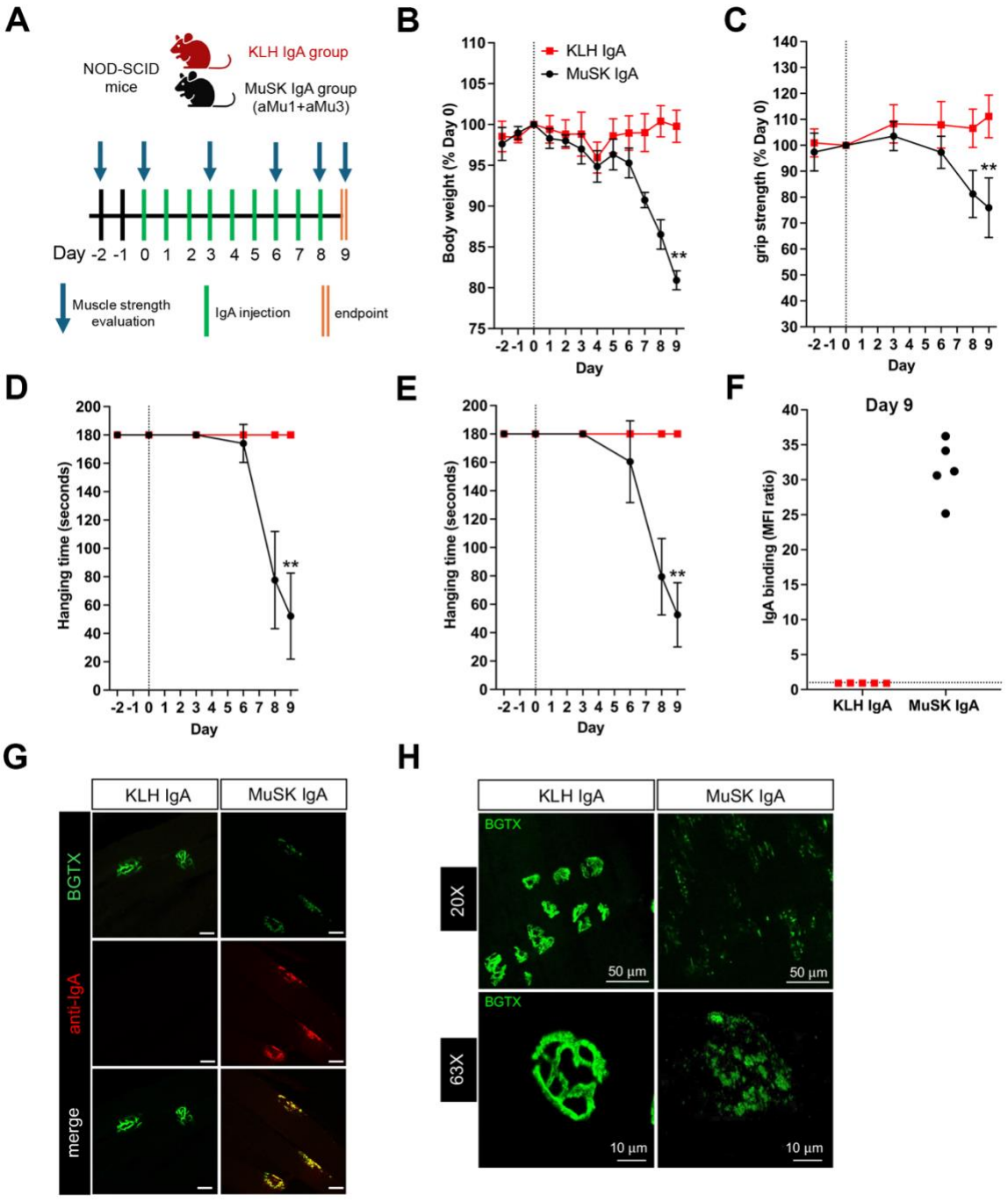
A
NOD-SCID mice
KLH IgA group
MuSK IgA group (aMu1+aMu3)
Day -2 -1 0 1 2 3 4 5 6 7 8 9
Muscle strength evaluation
IgA injection
endpoint
B
KLH IgA
MuSK IgA
Body weight (% Day 0)
Day
C
grip strength (% Day 0)
Day
D
Hanging time (seconds)
Day
E
Hanging time (seconds)
Day
F
Day 9
IgA binding (MFI ratio)
KLH IgA
MuSK IgA
G
KLH IgA
MuSK IgA
BGTX
anti-IgA
merge
H
KLH IgA
MuSK IgA
BGTX
20X
63X
50 µm
10 µm

Figure 7

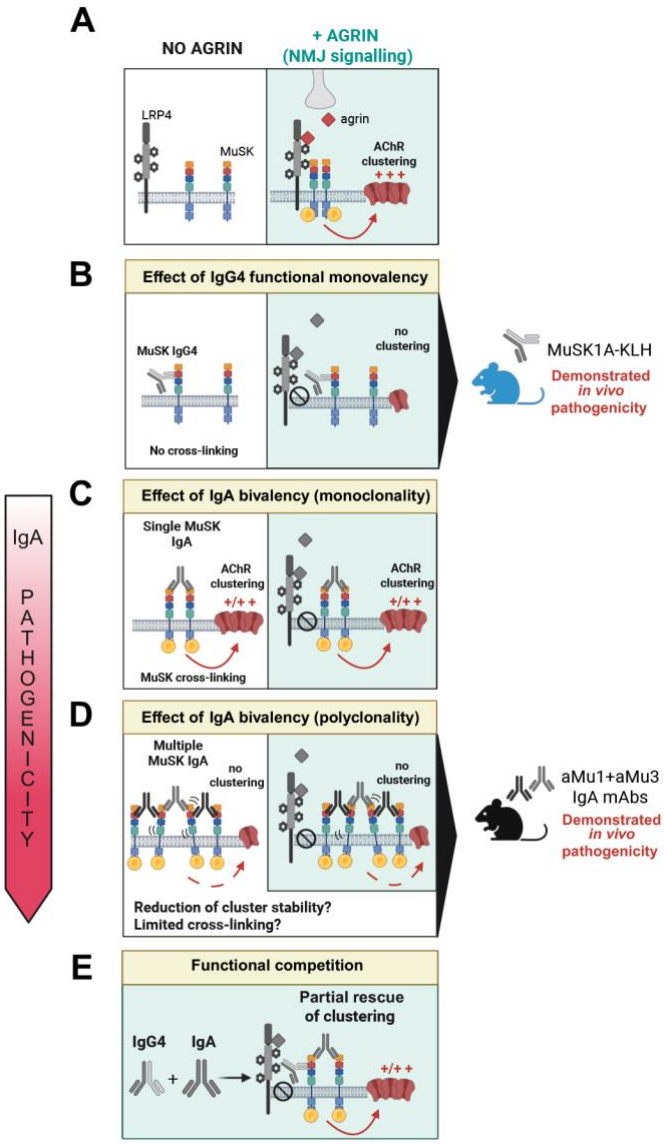
A
NO AGRIN
+ AGRIN
(NMJ signalling)
LRP4
MuSK
agrin
AChR
clustering
+ + +
B
Effect of IgG4 functional monovalency
MuSK IgG4
No cross-linking
no
clustering
MuSK1A-KLH
Demonstrated
in vivo
pathogenicity
C
Effect of IgA bivalency (monoclonality)
Single MuSK
IgA
AChR
clustering
+/+ +
MuSK cross-linking
AChR
clustering
+/+ +
IgA
PATHOGENICITY
D
Effect of IgA bivalency (polyclonality)
Multiple
MuSK IgA
no
clustering
no
clustering
Reduction of cluster stability?
Limited cross-linking?
aMu1+aMu3
IgA mAbs
Demonstrated
in vivo
pathogenicity
E
Functional competition
Partial rescue
of clustering
IgG4
IgA
+
+/+ +

Supplementary Information for

IgA autoantibodies demonstrate a novel mechanism of MuSK myasthenia gravis pathology

Gianvito Masi[1,2,*], Kangzhi Chen[1,3], Alexandra C. Bayer[1,2], Rafael Bayarri-Olmos[2], Minh C. Pham[2], Annabel Wallace[4], Silvia Falso[5], Amelia Evoli[5], Raffaele Iorio[5], Kenneth B. Hoehn[6], Akiko Iwasaki[2,7,8], Richard J. Nowak[1], and Kevin C. O'Connor[1,2,*]

This PDF includes:

- **Materials and Methods**

Materials and Methods

Human samples and ethical approval

This study was approved by the Human Investigation Committee at the Yale School of Medicine. Subjects' consent was obtained according to the Declaration of Helsinki. Serum and peripheral blood mononuclear cells (PBMCs) from patients with MuSK-MG, AChR-MG, healthy donors (HDs) and disease controls (neuromyelitis optica spectrum disorder and myelin oligodendrocyte glycoprotein antibody-associated disorder) were collected and cryopreserved in the Yale MG biorepository until retrieval for use. Additional MuSK MG sera were collected at Fondazione Policlinico Universitario Agostino Gemelli IRCCS in Rome, Italy. All patients fulfilled the diagnostic criteria for MG, including typical clinical presentations, compatible electrodiagnostic test results, and seropositivity for either MuSK or AChR autoantibodies measured via radioimmunoassay. The HDs had no reported history of autoimmune disorders, infections, malignancies or other major conditions.

Live cell-based assay for detecting autoantibodies using flow cytometry

The binding of MuSK, AChR and MOG autoantibodies was assessed with a live cell-based assay (CBA) as previously reported.[1] Briefly, HEK293T cells (ATCC, CRL3216) were transiently transfected with plasmids encoding MuSK-GFP, the four adult AChR subunits (2α, β, δ, and ε) and rapsyn-GFP (kindly provided by Drs. Angela Vincent, David Beeson, and Patrick Waters, Neurosciences Group at the Weatherall Institute of Molecular Medicine, University of Oxford) or MOG-GFP (kindly provided by Dr. Markus Reindl, Medical University of Innsbruck, Innsbruck, Austria) using branched polyethylenimine (Sigma, 408727). After 24 hours the media were changed, and on day 3 the cells were trypsinized, washed and seeded in 96-well U-bottom plates for autoantibody detection. Specifically, transfected cells were incubated with serum (1:100 diluted for IgA detection and 1:50 diluted for IgG detection), B-cell culture supernatants or monoclonal autoantibodies (mAbs) for 1 hour at 4°C with gentle shaking, washed with 1x PBS-1% BSA (Gibco, 14190144, Sigma, A9647-1006), and stained with a secondary Alexa-Fluor-647-conjugated rabbit anti-human-IgG-Fcγ antibody (1:1000, Jackson ImmunoResearch, 309-605-008) or Alexa-Fluor-647-conjugated goat anti-human serum IgAα antibody (1:1000, Jackson ImmunoResearch, 109-605-011) as needed, followed by three washes and flow cytometry testing on an LSR Fortessa (BD

Biosciences). The data were analyzed using FlowJo software (V10.10.0). For every sample tested, the median Alexa Fluor 647 fluorescence intensity (MFI) was measured in two cell populations: GFP-positive (antigen expression) and GFP-negative HEK293T cells (no antigen). The ratio between the two MFIs was calculated as follows: MFI_{GFP+} / MFI_{GFP-}. The MFI ratio values greater than 4 standard deviations (SD) above the mean of HD control group were regarded as positive. Serum samples from the discovery and the validation cohorts were tested following the same protocol. MuSK IgA screening was repeated for a subset of sera, following IgG depletion. Briefly, serum samples were diluted 1:2 with PBS and incubated overnight at 4°C with Protein G Sepharose beads (Cytiva, 17-0618-02) on a rotating shaker. The following day, samples were centrifuged for 15 minutes at 1500 rpm, and the supernatants were collected and re-incubated with Protein G beads for an additional 12 hours. A MuSK IgG CBA was performed to confirm depletion of MuSK IgG Abs, after which the IgG-negative fractions were re-screened for MuSK IgA Abs as previously described.

Validation of secondary antibody binding to IgA and IgG subclasses.

To verify the specificity of the secondary antibodies, we subcloned the VDJ segment of the MuSK-specific mAb MuSK1B[1] heavy chain into expression vectors encoding IgG1-4 (designed in our laboratory), IgA1 (kindly provided by Dr. David Martinez, Yale University) and IgM (kindly provided by Dr. Sarosh R. Irani, Mayo Clinic) backbones. The IgG and IgA mAbs were expressed and purified with Protein G Sepharose beads (Cytiva, 17-0618-02) and Peptide M (InvivoGen, gel-pdm-2), respectively. MuSK1B IgM was not purified but tested using the antibody-containing supernatants. In the live CBA, the binding of MuSK1B recombinantly expressed as IgG1-4, IgA1 and IgM was probed with the following secondary antibodies: Alexa-Fluor-647-conjugated rabbit anti-human-IgG-Fcγ (1:1000, Jackson ImmunoResearch, 309-605-008), Alexa-Fluor-647-conjugated goat anti-human serum IgAα (1:1000, Jackson ImmunoResearch, 109-605-011) or Alexa-Fluor-647-conjugated goat anti-human IgM-Fc5μ (1:1000, Jackson ImmunoResearch, 109-605-129).

B-cell culture for screening MuSK-specific clones

B cells were isolated from previously cryopreserved PBMCs by negative selection using the Human Pan B Cell Enrichment Kit (STEMCELL Technologies, 19554), followed by further

isolation of $CD27^+$ B cells using positive selection microbeads (Miltenyi Biotec, 130-051-601) together with MS Columns (Miltenyi Biotec, 130-042-201) and the MiniMACS™ Separator (Miltenyi Biotec, 130-042-102). The enriched $CD27^+$ B cells were distributed into 96-well flat-bottom plates with a density of less than 500 cells per well, and each well was pre-seeded with a layer of MS40L cells which express low levels of CD40L to support B cell activation (kindly provided by Drs. Garnett Kelsoe and Dongmei Liao, Duke University).[2] Cells were cultured at 37°C with 5% CO_2 in RPMI 1640 medium (Invitrogen, 11875093) in the presence of 10% fetal bovine serum (FBS) (Sigma, F0926), 1% penicillin-streptomycin (P/S) (100 U/mL) (Invitrogen, 15140122), 1% (10 mM) HEPES (Invitrogen, 15630080), 1% (1 mM) sodium pyruvate (Invitrogen, 11360070), 1% (100 μM) MEM NEAA (Invitrogen, 11140050), and 0.1% (55 μM) β-mercaptoethanol (Invitrogen, 21985023). In addition, culture supernatants were supplemented with 50 ng/mL IL-2 (Peprotech, 200-02), 10 ng/mL IL-4 (Peprotech, 200-04),10 ng/mL IL-21 (Peprotech, 200-21), and 10 ng/mL BAFF (Peprotech, 310-13) and replenished once a week to sustain B cell survival and antibody secretion.[2] After two weeks, supernatants were harvested and screened by a live CBA for MuSK-specific IgG and IgA binding using Alexa-Fluor-647-conjugated rabbit anti-human-IgG-Fcγ antibody (1:1000, Jackson ImmunoResearch, 309-605-008), PerCP-conjugated goat anti-human-IgAα antibody (1:100, Jackson ImmunoResearch, 109-125-011) or Alexa-Fluor-647-conjugated goat anti-human serum IgAα (1:1000, Jackson ImmunoResearch, 109-605-011). The B cells from the wells containing MuSK IgA autoantibodies were harvested and subcultured at a density of less than three cells per well for an additional three weeks. The supernatants and cells from the wells containing MuSK IgG autoantibodies were collected and cryopreserved for future investigations. After three weeks, the B cell supernatants were retested for MuSK IgA autoantibodies, and the B cells from the positive wells identified in this screening were harvested for downstream RNA isolation and mAb cloning.

Molecular cloning of MuSK-specific IgA mAbs

The recombinant mAbs were produced as previously reported with modifications.[1,3] Briefly, MuSK-specific B cells identified by the B-cell culturing strategy described above were harvested and lysed for RNA isolation using a commercial kit (Qiagen, 74104) according to manufacturer's instructions, followed by cDNA synthesis with random hexamers (Invitrogen, N8080127), dNTP mix (Invitrogen, 18427088), and SuperScript III reverse transcriptase (Invitrogen, 18080044). The resulting cDNA was then subjected to a two-step nested

polymerase chain reaction (PCR) to specifically amplify the V(D)J regions, as previously described[4], except one modification: to clone IgA B cells, in the first PCR round we employed an IgA-specific reverse primer that anneals to a common sequence shared by the IgA1 and IgA2 constant regions (5'-CTTTCGCTCCAGGTCACACTGAG-3'). The purified PCR products were subcloned into human IgA1, Igκ and Igλ expression vectors as appropriate. The recombinant plasmids with verified V(D)J sequences were used for mAb expression. To this end, HEK293A cells were cultured in serum-free basal media — consisting of 48% DMEM (Invitrogen, 11995065), 48% RPMI 1640 medium (Invitrogen, 11875093), 1% antibiotic/antimycotic (Invitrogen, 15240062), 1% sodium pyruvate (Invitrogen, 11360070) — supplemented with 1% Nutridoma-SP (Roche, 11011375001). Cells were transfected with an equal mass (5 μg) of paired heavy and light chain plasmids via linear polyethylenimine (Polysciences, 23966) (PEI/DNA ratio 2:1) in a 10-cm dish, and after 5-6 days the supernatants were collected and assessed for the presence of MuSK autoantibody via a live CBA. The supernatants with confirmed MuSK IgA positivity were subjected to IgA purification with Peptide M (InvivoGen, gel-pdm-2). A dimeric IgA mAb (aMu1) was expressed by transfecting HEK293A cells with plasmids encoding paired aMu1 heavy and light chains, together with a J-chain expressing plasmid (Addgene, Plasmid #14514), at a 1:1:1 ratio. Correct size and purity were evaluated by SDS-PAGE. The VDJ segments of five clonal variants identified through BCR-seq were subcloned into an IgA1 vector and recombinantly paired with the native light chain of the original mAb, followed by recombinant mAb expression and validation of mAb binding with CBA as described above.

IgA subclass determination

To determine the specific IgA subclass of each MuSK IgA mAb, a custom two-step nested PCR that utilized the known variable regions was designed. Specifically, PCR1 was run with a reverse primer that annealed to a common CH2 domain in both IgA1 and IgA2 constant regions. In the subsequent PCR2, the forward primer captured the specific HCDR3 region of each IgA mAb, and the reverse primer annealed to a common CH2 domain in both IgA1 and IgA2 but further nested compared to the PCR1 reverse primer. This PCR2 reverse primer was used to sequence the resulting PCR2 product. The IgA subclass was determined by examining the sequence encoded by the hinge region. IgA1 hinge region:(5'CCAGTTCCCTCAACTCC ACCTACCCCATCTCCCTCAACTCCACCTACCCCATCTCCCTCATGC-3'; IgA2 hinge region: (5'-CCAGTTCCCCCACCTCCCCCATGC-3').[5]

Immunoglobulin sequence analysis

The sequences of heavy and light chain variable regions were aligned to reference immunoglobulin genes the IMGT/V-QUEST software [program version 3.6.3 (30 January 2024) - IMGT/V-QUEST reference directory release: 202430-2 (23 July 2024)].[6] Germline gene usage and somatic mutations leading to nonsynonymous substitutions (replacements) were inferred by the IMGT/V-QUEST program. The N-glycosylation sites in the variable region were identified by manually counting the consensus sequence N-X-S/T, for which X represents any amino acid except proline.

MuSK IgA mAb testing

The MuSK-specific IgA mAbs were tested for binding on live MuSK cell-based assay using a concentration range from 1 μg/mL to 0.0014 μg/mL, with 3-fold serial dilutions in between these endpoints. The live CBA was performed as described above. MuSK1B,[1] a patient-derived MuSK-specific IgG3 mAb, was recombinantly re-expressed as an IgA1 antibody and used as a positive control. In addition, an AChR-specific human mAb, mAb01a,[3] subcloned into the IgA1 vector was used as a negative control. To test binding to murine MuSK, patient-derived IgA mAbs were incubated with HEK293T cells transfected with a plasmid encoding mouse MuSK fused extracellularly to a DYKDDDDK tag (kindly provided by Dr. Justin Fallon). Ab binding was then revealed using Alexa-Fluor-647-conjugated goat anti-human serum IgAα (1:1000, Jackson ImmunoResearch, 109-605-011), whereas mouse MuSK expression was detected with a rabbit anti-DDK monoclonal antibody (Clone: D6W5B, Cell Signaling Technology), followed by Alexa-Fluor-647 Goat Anti-Rabbit IgG, Fc fragment specific (1:1000, Jackson ImmunoResearch,109-545-008). All mAbs were tested at a concentration of 1 μg/mL.

Microscopy-based indirect immunofluorescence

The MuSK IgA binding measured by CBA using flow cytometry was complemented with microscopy-based indirect immunofluorescence. HEK293T cells were seeded on polylysine-D-coated coverslips and transfected with the MuSK-GFP plasmid as described above. Cells were incubated with either mAbs (1 μg/mL) or serum samples (1:50 for IgG detection, 1:100 for IgA detection) diluted in cell media at room temperature for 1 hour, washed three times with 1x PBS, fixed with 4% paraformaldehyde (BioLegend, 420801) for 8 minutes, and

blocked with 10% normal goat serum (NGS) in 1x PBS for 20 minutes. For IgG and IgA detection, cells were incubated with Alexa-Fluor-647-conjugated rabbit anti-human-IgG-Fcγ (1:1000, Jackson ImmunoResearch, 309-605-008) or Alexa-Fluor-647-conjugated goat anti-human serum IgAα (1:1000, Jackson ImmunoResearch, 109-605-011) secondary antibodies diluted in 10% NGS for 1 hour. After three washes with 1x PBS/Tween 1%, the coverslips were mounted using Vectashield Vibrance antifade mounting medium with DAPI (Vector Laboratories, H-1800-2). Images were captured at a 63× magnification (zoom: 3) using a SP8 confocal laser-scanning microscope with Las X software (Leica).

MuSK-domain mapping assay

To determine the domain specificity of the MuSK-IgA mAbs, their VDJ segments were subcloned into an IgG1 vector since the control mAbs (each binding to a different MuSK domain) had already been expressed using an IgG1 or IgG4 backbones. Different human MuSK domain expression constructs (Ig-like 1, Ig-like 2, and frizzled-like domains) were generated as previously shown.[1] The binding to HEK293T cells transfected with plasmids encoding single MuSK domains was detected via CBA. MuSK-specific mAbs 2E6 (previously demonstrated to be a Ig-like 1 domain binder),[7] MuSK1B (Ig-like 2 domain binder),[1] and a humanized murine MuSK-specific mAb 4A3 (frizzled-like domain binder)[8] were used as positive controls. In addition, mAb09, an AChR-specific mAb,[3] was used as a negative control. For the "no mAb" condition, only the secondary antibody was added. All mAbs were tested at a concentration of 1 μg/mL.

MuSK binding competition assay

To assess whether the MuSK-specific IgA mAbs competed for MuSK binding with our previously identified MuSK-specific IgG4 mAbs, MuSK-GFP-transfected HEK293T cells were first incubated with either FACS buffer (non-competing condition), the three MuSK-specific IgA mAbs or an AChR-specific mAb (mAb01a,[3] subcloned into an IgA1 backbone) at an excess concentration (10 μg/mL) — to saturate the available binding sites— for 45 minutes. After 2 washes, cells were incubated with MuSK1A,[1] 2E6,[7] and 6C6[7] bivalent IgG4 mAbs at a concentration of 0.5 μg/mL, re-washed and subsequently incubated with Alexa-Fluor-647-conjugated rabbit anti-human-IgG-Fcγ antibody (1:1000, Jackson ImmunoResearch, 309-605-008) and analyzed with flow cytometry.

Detection of antibody J chain by cell-based assay

MuSK-GFP-expressing HEK293T cells were incubated with serum samples (1:10 dilution) or IgA mAbs (1 ug/ml). The J chain of serum antibodies or mAbs binding to MuSK was detected with a J chain-specific mouse monoclonal antibody (clone: F-12, Santa Cruz Biotechnology), followed by an APC anti-mouse IgG_{2a} secondary antibody (Cat. 407110, BioLegend). Binding was measured using flow cytometry.

Estimation of absolute levels of MuSK autoantibodies.

To enable quantification of MuSK IgG4 and IgA Abs in serum samples, MuSK1B, a MuSK-specific recombinant mAb, was expressed as an IgA1 and IgG4 mAb. Serum samples were serially diluted and tested for IgA and IgG4 binding on a MuSK CBA. MuSK1B IgA1 and IgG4 mAbs were used to generate standard curves to allow quantification of absolute levels of the respective subclass in each sample.

AChR clustering assay

The AChR clustering assay was performed as previously reported,[7] with few modifications. Briefly, mouse C2C12 myoblasts (ATCC, CRL-1772) were seeded in 96-well flat-bottom plates at a density of 10,000 cells per well and cultured in growth media consisting of DMEM-GlutaMAX (Invitrogen, 10566016) with 10% FBS (Sigma, F0926) and 1% P/S (100 U/mL) (Invitrogen, 15140122). When cells were confluent, the growth media were then switched to differentiation media (DM) prepared with DMEM-GlutaMAX (Invitrogen, 10566016), 2% horse serum (Gibco™, 16050122), and 1% P/S (100 U/mL) (Invitrogen, 15140122) to induce myotube differentiation. The DM was changed every other day, until evident fusion of myotubes was observed. AChR clustering was induced with 10 ng/mL rat agrin (R&D Systems, 550-AG) for 24 hours. 8-18C5, a humanized MOG-specific mAb,[9] was subcloned into an IgA1 vector and used as a negative control. All mAbs were tested at 1 µg/ml for 24 hours, in the presence or absence of agrin. In additional experiments, the IgA mAbs or 8-18C5 IgA and our previously established MuSK-specific IgG4-derived Fabs (MuSK1A, 6C6 and 2E6) were co-incubated at equimolar concentration (1 µg/ml for mAbs and 0.3 µg/ml for Fabs) in the presence of agrin. The rescue effect of each IgA mAb (percentage) was calculated using the following formula: $[(\text{agrin} + \text{IgA mAb} + \text{Fab}) - (\text{agrin} + \text{Fab})]/(\text{agrin only} - \text{untreated})$. The IgA mAbs were also tested in combinations with and without agrin. To allow subsequent comparisons and analysis, all experimental conditions were always run side-by-

side. After 24 hours, cells were incubated with Alexa-Fluor-488-conjugated alpha-bungarotoxin (Invitrogen, B13422) diluted 1:1000 in DM at 37°C for 1 hour, washed for three times with 1x PBS, and fixed with 4% paraformaldehyde (BioLegend, 420801) for 20 minutes in the dark at room temperature. Myotubes were visualized at a 20× magnification with a Leica DMi8 fluorescence microscope. For each well, three visual fields with fully differentiated myotubes were selected on brightfield, and images were captured on fluorescence. Each condition was tested in duplicate wells as technical replicates, and at least three repetitions were performed as biological replicates. AChR clusters greater than 15 μm^2, considered as mature and the most functionally relevant clusters,[10] were counted with ImageJ software.[11] The number of clusters from two wells was averaged and normalized to the effect of agrin in each experiment.

MuSK tyrosine phosphorylation assay

MuSK tyrosine phosphorylation was determined as previously described.[1] In brief, differentiated C2C12 myotubes on 6-well plates were stimulated with 10 ng/mL rat agrin (R&D Systems, 550-AG) and/or 1 μg/mL mAbs (the MuSK-specific IgA mAbs and the MOG-specific 8-18C5 IgA) for 30 minutes at 37°C. After stimulation, myotubes were washed with ice-cold 1x PBS and lysed in 250 μL RIPA buffer (Invitrogen, 89900) containing protease inhibitor (Invitrogen, A32957) and phosphatase inhibitor (Invitrogen, A32953) with rotation for 30 minutes at 4°C, followed by 20 minutes of centrifugation at 10,000 g to pellet the insoluble fractions. The whole-cell lysates were incubated with 5 μL (1 μg) goat anti-rat polyclonal MuSK antibody (R&D Systems, AF562) with rotation at 4°C overnight, and the antibody binding to MuSK was captured by co-incubation with Dynabeads Protein G (Invitrogen, 10003D) for 1 hour at 4°C. Beads-precipitated protein complexes were eluted using 20 μL Laemmli sample buffer (Bio-Rad, 1610737) with the addition of reducing agent β-mercaptoethanol (Sigma, M3148) and boiled at 100°C for 10 minutes, loaded for SDS-PAGE and transferred onto polyvinylidene fluoride (PVDF) membranes. After blocking with TBST (Bio-Rad, BUF028) containing 3% BSA (Sigma, A9647-1006) at room temperature for 1 hour, membranes were incubated with 1:1000-diluted mouse anti-phosphotyrosine primary antibody (clone 4G10, Sigma-Aldrich, 05-321) at 4°C overnight, washed 3 times, and incubated with 1:20000-diluted (0.05 μg/mL) goat anti-mouse IgG (H+L) cross-adsorbed HRP-conjugated secondary antibody (Invitrogen, G-21040) at room temperature for an hour. The membranes were then developed by chemiluminescent detection with Clarity™ Western ECL Substrate

(Bio-Rad, 1705060) and were stripped under harsh conditions (in 62.5 mM Tris-HCl buffer at pH 6.8, containing 2% SDS and 0.8% β-mercaptoethanol). To reprobe for MuSK, membranes were blocked, incubated with 1:1000-diluted (0.2 µg/mL) goat anti-rat MuSK antibody (R&D, AF562) at 4°C overnight, washed 3 times, and incubated with 1:5000-diluted (0.2 µg/mL) rabbit anti-goat IgG (H+L) cross-adsorbed HRP-conjugated secondary antibody (Invitrogen, R-21459) for an hour at room temperature. Densitometry of all the blots was analyzed using ImageJ software. For each condition, the level of MuSK phosphorylation was normalized to immunoprecipitated MuSK. The ratio of phosphorylated to total MuSK was then normalized to the agrin effect.

Bulk B cell repertoire sequencing

Bulk B cell repertoire (BCR) libraries were prepared as previously reported.[7] RNA was isolated from approximately 10 million cryopreserved PBMCs using the RNeasy Mini Kit (Qiagen, 74134). BCR libraries were generated using the SMART-Seq Human BCR (with UMIs) kit (Takara Bio Inc., 634777) according to the manufacturer's instructions. Briefly, first-strand cDNA synthesis from isolated RNA was primed by the dT primer, and SMART UMI Oligo was used for template switching at the 5' end of the transcript. Then a two-step semi-nested PCR was performed to amplify the entire V(D)J region and a portion of the constant regions of BCR cDNA. The hBCR Universal Forward primer that anneals to the SMART UMI oligo sequence and incorporates the Illumina Read 2 sequence was used for PCR1, where a mixture of reverse primers for IgA/D/E/G/M heavy chains and IgK/L light chains that anneal to sequences in the constant regions of human BCR heavy-chain and light-chain cDNA were used. For PCR2, the Unique Dual Index primers that anneal to a sequence added by hBCR PCR1 Universal Forward primer and incorporate the Illumina P7-i7 index sequences, and hBCR PCR2 HC Reverse primers that anneal to sequences in BCR constant regions internal to sequences bound by the reverse primers for PCR1 and incorporate both the Illumina Read 1 and P5-i5 index sequences were used. PCR-amplified libraries are then purified by immobilization on NucleoMag NGS Clean-up and Size Select beads. After quality analysis, twelve libraries containing 4 nM DNA were pooled in equimolar amounts for sequencing on the Illumina MiSeq, with 20% PhiX control spike-in.

B-cell receptor sequence processing and B-cell clonal analysis

Bulk and single cell B-cell receptor sequencing data from MuSK-1 and MuSK-2 were obtained from previously processed datasets[7] and newly generated sequences with the Takara SMART-Seq Human BCR kit. All BCR repertoire sequencing data were analyzed using the Immcantation (www.immcantation.org) framework. BCR sequences from all data sources were pooled together with the heavy chain sequence of aMu1. Nonproductive heavy chains were removed, and light chain sequences were excluded from clonal clustering analysis. To limit low-coverage sequences, all sequences with fewer than 300 unambiguous nucleotide characters (ATCG) were discarded. Novel IGHV alleles and subject-specific IGHV genotypes were inferred using TIgGER v1.0.0.[12] To identify B cell clones, sequences were first partitioned based on common V and J gene annotations, as well as junction length. Within these groups, sequences differing from one another by a Hamming distance threshold of 0.11 within the junction region were clustered into clones using single linkage hierarchical clustering,[13,14] implemented in Scoper v1.3.0.[15] This Hamming distance threshold was determined by finding the local minimum between modes of the distance to the nearest sequence neighbor plot using shazam v1.2.0.[16] Unmutated germline V and J gene sequences were then reconstructed for the clone containing aMu1 using the createGermlines function within Dowser v2.3.0.[17] The lineage tree of this clone was built using IgPhyML v2.0.0[18] and Dowser v2.3.0.[17] More specifically, the tree topology, branch lengths, and substitution model parameters were estimated first under the GY94 model[19] and then branch lengths and substitution model parameters under the HLP19 model.[18] Trees were visualized using Dowser v2.3.0, ggtree v3.10.1,[20] and ggplot v3.5.1.[21] Measurable evolution was determined by a date randomization test in which the correlation between divergence (sum of branch lengths to the germline) and sample date of each tip is compared to the same statistic with the tip date randomized.[22] This was performed using the correlationTest function in Dowser, with a null distribution of 100,000 uniform permutations. All B cell clonal analyses were performed using R v4.4.1.

Scripts for performing B cell receptor sequence processing and analyses are available https://github.com/hoehnlab/publication_scripts.

Generation of MuSK1A-KLH, a functionally monovalent, MuSK-specific monoclonal autoantibody

A functionally monovalent MuSK mAb was generated by incorporation of an anti-keyhole limpet hemocyanin (KLH) antibody arm in MuSK1A (a human-derived MuSK mAb), using a controlled Fab-arm exchange process.[23] Parental IgG1 antibodies containing single matching

point mutations in the CH3 domain were mixed at a 1:1 molar ratio, adjusted to 1 mg/mL in 1x PBS (pH 7.4), and reduced with a final concentration of 25 mM 2-mercaptoethylamine•HCl. Samples were incubated for 3 hours at room temperature, and reduction efficiency was confirmed using SDS-PAGE. The reducing agent was removed using 40k Zeba Desalting Spin columns pre-equilibrated in 1x PBS (pH 7.4), and the samples were allowed to re-oxidize overnight at 4 °C. The controlled Fab-arm exchange reaction was assessed using intact mass analysis to confirm reassembled monovalent antibody, SEC-HPLC (>95% main peak), and SDS-PAGE for purity.

Expression of patient-derived monoclonal mAbs for passive transfer experiments

For passive immunization experiments, monoclonal antibodies were expressed in Expi-293 cells using the Expi293™ Expression System Kit (Thermo Fisher), according to the manufacturer's instructions. Following protein expression, IgA antibodies were purified with Peptide M (InvivoGen, gel-pdm-2) and eluted with sterile 0.1 M glycine (pH 3.0; cat. G4530, teknova). pH was immediately neutralized using 1 M Tris-HCl (pH 8.0; cat. T1080, teknova). 1x PBS buffer exchange was achieved using Amicon Ultra centrifugal filters (Merck Millipore) through a 50-kDa membrane according to the manufacturer's instructions. Endotoxin measurement was performed with the limulus amebocyte lyasate kit (PTS20F, Charles River), according to the manufacturer's instructions. Antibody concentrations were measured by ELISA.

Mouse Passive immunization experiments

Female 5-to-6-week-old NOD.Cg-Prkdcscid/J (NOD/SCID) mice were purchased from the Jackson Laboratory. All mice were subsequently bred and housed at Yale University. All procedures used in the present study complied with federal guidelines and the institutional policies of the Yale School of Medicine Animal Care and Use Committee. No statistical methods were used to predetermine the sample size, but our sample sizes were similar to those of a previous publication.[24] Randomization was used to allocate each mouse to either the control or treatment groups. Each experimental group consisted of 5 mice, and each cage housed mice from the control and the treatment groups to minimize potential confounding effects. The experimenters were blinded for the injected antibodies throughout all experiments

and analyses. To assess the pathogenicity of MuSK1A-KLH, mice received an intraperitoneal injection of 1 mg/kg recombinant antibody (MuSK1A-KLH or KLH IgG), every 3 days (day 0, 3 and 6). In this pilot experiment, a group of untreated mice was included as an additional control. To investigate the pathogenicity of MuSK IgA Abs, mice received either a mixture of two MuSK IgA mAbs (aMu1 + aMu3 in 1:1 ratio) or KLH IgA (5 mg/kg of total antibody). Given the shorter half-life of IgA compared to that of IgG,[25] injections were performed on a daily basis to ensure continuous IgA exposure. In both experiments, body weight was measured daily. Muscle strength was evaluated every three days, unless otherwise specified. Peak grip strength force was measured with the 47200 Grip Strength Meter, and four measurements per mouse were recorded during each assessment. In vivo muscle strength and endurance were also evaluated with two hanging tests, using an inverted mesh and a rolling loop, as described elsewhere.[24,26] Mice were euthanized if they lost ≥20% of their body weight compared to the first day of injection or upon reaching the end of the experiment.

Whole-mount muscle immunostaining

The mouse diaphragm and epitrochleoanconeus (ETA) were dissected, rinsed once in 1x PBS, pinned and fixed with 1x PBS/PFA 1% at RT for 30 minutes. Following fixation, muscles were washed three times with 1x PBS, incubated with 0.1M glycine for one hour at RT and re-washed. The whole ETA and the diaphragm (cut in smaller sections) were then permeabilized and blocked for two hours at RT in blocking buffer (1x PBS/BSA 2%/Triton X-100 1%). For labelling of NMJs, muscles were stained with Alexa-Fluor-488-conjugated alpha-bungarotoxin (Invitrogen, B13422) for two hours at RT. Finally, muscles were washed with 0.1% Triton X-100 for three hours and mounted on slides in Vectashield Vibrance antifade mounting medium with DAPI (Vector Laboratories, H-1800-2). For IgA detection, muscles were first incubated overnight with Alexa-Fluor-647 anti-human IgA (Jackson ImmunoResearch, 109-605-011; 1:1000 in blocking buffer). After several washes with 1x PBS-Triton X-100 0.1%, muscles were stained with bungarotoxin as previously described. Images of the neuromuscular junctions were acquired on a SP8 confocal laser-scanning microscope with Las X software (Leica).

Statistics

Analyses were performed using GraphPad Prism software (version 10.3.0). For all experiments, the normality of the data was assessed via the Shapiro-Wilk test. According to

the data distribution, the differences among three or more groups were analyzed with ordinary one-way ANOVA followed by the Dunnett's multiple comparison test or the Kruskal-Wallis test followed by the Dunn's multiple comparisons test. Comparisons between two groups were analyzed using a two-tailed unpaired t test. A significance threshold of $P < 0.05$ was used. Correlation analyses were performed using the Spearman's rank correlation test or Pearson correlation coefficient, as appropriate. To depict the relationship between variables, a simple linear regression was performed.

References

1. Takata K, Stathopoulos P, Cao M, et al. Characterization of pathogenic monoclonal autoantibodies derived from muscle-specific kinase myasthenia gravis patients. *JCI Insight*. Jun 20 2019;4(12):e127167. doi:10.1172/jci.insight.127167

2. Su K-Y, Watanabe A, Yeh C-H, Kelsoe G, Kuraoka M. Efficient Culture of Human Naive and Memory B Cells for Use as APCs. *Journal of Immunology (Baltimore, Md : 1950)*. 2016;197(10):4163-4176.

3. Pham MC, Masi G, Patzina R, et al. Individual myasthenia gravis autoantibody clones can efficiently mediate multiple mechanisms of pathology. *Acta Neuropathol*. Aug 2023;146(2):319-336. doi:10.1007/s00401-023-02603-y

4. Wardemann H, Yurasov S, Schaefer A, Young JW, Meffre E, Nussenzweig MC. Predominant autoantibody production by early human B cell precursors. *Science (New York, NY)*. 2003;301(5638):1374-1377.

5. Woof JM, Kerr MA. The function of immunoglobulin A in immunity. *The Journal of Pathology*. 2006;208(2):270-282.

6. Brochet X, Lefranc M-P, Giudicelli V. IMGT/V-QUEST: the highly customized and integrated system for IG and TR standardized V-J and V-D-J sequence analysis. *Nucleic Acids Res*. 2008;36(Web Server issue):W503-W508. doi:10.1093/nar/gkn316

7. Fichtner ML, Hoehn KB, Ford EE, et al. Reemergence of pathogenic, autoantibody-producing B cell clones in myasthenia gravis following B cell depletion therapy. *Acta Neuropathol Commun*. Oct 28 2022;10(1):154. doi:10.1186/s40478-022-01454-0

8. Stathopoulos P, Kumar A, Nowak RJ, O'Connor KC. Autoantibody-producing plasmablasts after B cell depletion identified in muscle-specific kinase myasthenia gravis. *JCI Insight*. Sep 07 2017;2(17):e94263-e94275. doi:10.1172/jci.insight.94263

9. Linnington C, Webb M, Woodhams PL. A novel myelin-associated glycoprotein defined by a mouse monoclonal antibody. *J Neuroimmunol*. Sep-Oct 1984;6(6):387-96. doi:10.1016/0165-5728(84)90064-x

10. Lim JL, Augustinus R, Plomp JJ, et al. Development and characterization of agonistic antibodies targeting the Ig-like 1 domain of MuSK. *Sci Rep*. May 8 2023;13(1):7478. doi:10.1038/s41598-023-32641-1

11. Schneider CA, Rasband WS, Eliceiri KW. NIH Image to ImageJ: 25 years of image analysis. *Nat Methods*. 2012;9(7):671-675.

12. Gadala-Maria D, Yaari G, Uduman M, Kleinstein SH. Automated analysis of high-throughput B-cell sequencing data reveals a high frequency of novel immunoglobulin V gene segment alleles. *Proceedings of the National Academy of Sciences of the United States of America*. 2015;112(8):E862-E870. doi:10.1073/pnas.1417683112

13. Gupta NT, Vander Heiden JA, Uduman M, Gadala-Maria D, Yaari G, Kleinstein SH. Change-O: a toolkit for analyzing large-scale B cell immunoglobulin repertoire sequencing data. *Bioinformatics (Oxford, England)*. 2015;31(20):3356-3358. doi:10.1093/bioinformatics/btv359

14. Gupta NT, Adams KD, Briggs AW, Timberlake SC, Vigneault F, Kleinstein SH. Hierarchical Clustering Can Identify B Cell Clones with High Confidence in Ig Repertoire Sequencing Data. *Journal of Immunology (Baltimore, Md : 1950)*. 2017;198(6):2489-2499. doi:10.4049/jimmunol.1601850

15. Nouri N, Kleinstein SH. A spectral clustering-based method for identifying clones from high-throughput B cell repertoire sequencing data. *Bioinformatics*. 2018;34(13):i341-i349. doi:10.1093/bioinformatics/bty235

16. Yaari G, Vander Heiden JA, Uduman M, et al. Models of somatic hypermutation targeting and substitution based on synonymous mutations from high-throughput

immunoglobulin sequencing data. *Frontiers In Immunology*. 2013;4:358. doi:10.3389/fimmu.2013.00358

17. Hoehn KB, Pybus OG, Kleinstein SH. Phylogenetic analysis of migration, differentiation, and class switching in B cells. *PLoS Comp Biol*. 2022;18(4):e1009885. doi:10.1371/journal.pcbi.1009885

18. Hoehn KB, Vander Heiden JA, Zhou JQ, Lunter G, Pybus OG, Kleinstein SH. Repertoire-wide phylogenetic models of B cell molecular evolution reveal evolutionary signatures of aging and vaccination. *Proceedings of the National Academy of Sciences of the United States of America*. 2019;116(45):22664-22672. doi:10.1073/pnas.1906020116

19. Nielsen R, Yang Z. Likelihood models for detecting positively selected amino acid sites and applications to the HIV-1 envelope gene. *Genetics*. 1998;148(3):929-936.

20. Yu G, Lam TT-Y, Zhu H, Guan Y. Two Methods for Mapping and Visualizing Associated Data on Phylogeny Using Ggtree. *Mol Biol Evol*. 2018;35(12):3041-3043. doi:10.1093/molbev/msy194

21. Wickham H. *ggplot2: Elegant Graphics for Data Analysis*. Springer; 2016.

22. Hoehn KB, Turner JS, Miller FI, et al. Human B cell lineages associated with germinal centers following influenza vaccination are measurably evolving. *Elife*. Nov 17 2021;10doi:10.7554/eLife.70873

23. Linnington C, Webb M, Woodhams PL. A novel myelin-associated glycoprotein defined by a mouse monoclonal antibody. *J Neuroimmunol*. 1984;6(6):387-396.

24. Vergoossen DLE, Plomp JJ, Gstöttner C, et al. Functional monovalency amplifies the pathogenicity of anti-MuSK IgG4 in myasthenia gravis. *Proceedings of the National Academy of Sciences of the United States of America*. 2021;118(13)doi:10.1073/pnas.2020635118

25. Vieira P, Rajewsky K. The half-lives of serum immunoglobulins in adult mice. *Eur J Immunol*. Feb 1988;18(2):313-6. doi:10.1002/eji.1830180221

26. Hoffman E, Winder SJ. A Modified Wire Hanging Apparatus for Small Animal Muscle Function Testing. *PLoS Curr*. May 2 2016;8doi:10.1371/currents.md.1e2bec4e78697b7b0ff80ea25a1d38be

Supplementary Information for

IgA autoantibodies demonstrate a novel mechanism of MuSK myasthenia gravis pathology

This PDF file includes:

Supplementary Table 1. Demographic, clinical, and laboratory data of MuSK MG patients harboring MuSK IgA autoantibodies.

Patient ID	Sex	Age at TOC	Time (months) since first TOC	MGFA Class	MG-ADL and MGC score at TOC	Time since last RTX (months)	Concomitant immuno-therapies	MuSK IgG titer (CBA)	MuSK IgA titer (CBA)	Origin of clone or clonal variant
MuSK-1-1	F	60	0	IIb	NA; 3	28	None	>1:20480	<1:100	-
MuSK-1-2	F	61	18	0	NA; 0	1	None	>1:20480	<1:100	-
MuSK-1-3	F	62	26	0	NA; 0	9	None	1:1280	<1:100	-
MuSK-1-4	F	62	31	0	NA; 0	14	None	>1:20480	<1:100	-
MuSK-1-5	F	63	36	0	NA; 0	19	None	>1:20480	<1:100	1 CV of 2E6 IgG4
MuSK-1-6	F	63	38	IIb	NA; 7	21	None	>1:20480	<1:100	-
MuSK-1-7	F	63	44	0	NA; 0	5	None	1:5120	<1:100	-
MuSK-1-8	F	64	50	0	NA; 0	1	None	1:5120	<1:100	-
MuSK-1-9*	F	65	61	0	NA; 0	12	None	1:10240	1:160	4 CVs of aMu1 IgA
MuSK-1-10*	F	65	68	0	NA; 0	19	None	>1:20480	1:320	1 CV of 2E6 IgG4
MuSK-1-11*	F	65	69	IIb	NA.; 7	20	PD	>1:20480	1:160	2E6 IgG4; 1 CV of 2E6 IgG4; 2 CVs of aMu1 IgA
MuSK-1-12*	F	65	78	0	NA; 0	3	None	1:5120	1:160	5 CVs of aMu1 IgA
MuSK-1-13*	F	70	127	IIa	5, 9	26	PD	>1:20480	1:640	aMu1 IgA; 9 CVs of aMu1 IgA
MuSK-1-14*	F	71	138	0	0,0	3	None	1:640	1:160	4 CVs of aMu1 IgA
MuSK-2-1*	F	33	0	0	NA; 0	-	MM	>1:20480	1:160	aMu2 IgA; 1 CV of aMu2
MuSK-2-2	F	35	24	IIb	NA; 13	-	MM	>1:20480	<1:100	-
MuSK-2-3	F	36	35	IIb	NA; 4	11	MM	<1:50	<1:100	-
MuSK-3-1*	F	47	0	0	-	15	PD	>1:20480	1:100	aMu3 IgA
MuSK-4-1*	F	40	0	IIb	6;18	-	PD	>1:20480	1:320	-
MuSK-4-2*	F	40	1	0	1;10	-	PD, RZX	>1:20480	1:160	-
MuSK-4-3*	F	40	2	IIb	7;17	-	PD	>1:20480	1:160	-
MuSK-4-4*	F	40	3	0	1;9	-	PD, RZX	>1:20480	1:160	-

Four MuSK MG patients (MuSK-1, MuSK-2, MuSK-3 and MuSK-4) tested positive for MuSK-specific IgA by cell-based assay (CBA). For each patient, the table includes longitudinal samples indicated by a progressive number (-1,-2, etc.) following the patient ID. MuSK IgA seropositive samples are indicated with an asterisk. CBA end-point titers were measured using flow cytometry (positivity cutoff for IgA ≥1:100; positivity cutoff for IgG ≥ 1:50). MuSK-specific IgA B cells were isolated from the following timepoints: MuSK-1-13; MuSK-2-1; MuSK-3-1. Clonal variants of isolated MuSK-specific IgA B cells were identified using bulk B-cell receptor sequencing analysis and are shown in the last column. For samples belonging to MuSK-4, MG-ADL and QMG scores are shown. CBA: cell-based assay; CV: clonal variant; F: female; MG-ADL: Myasthenia Gravis Activities of Daily Living; MGC: Myasthenia Gravis Composite; MGFA: Myasthenia Gravis Foundation of America; MuSK: muscle-specific tyrosine kinase; MM: mycophenolate mofetil; n.a.: not available; PD: prednisone; RZX: rozanolixizumab; TOC: time of collection.

Supplementary Table 2. Comparison of the clinical characteristics of MuSK IgA seropositive and seronegative MG patients.

	MuSK IgA Pos (n=4) (%)	MuSK IgA Neg (n=35) (%)	*p* value*
Female	4/4 (100)	28/35 (80)	>0.9999
Median age at onset (IQR range)	40.5 (33.8-56.3)	35 (23-73)	0.3884
Clinical presentation at onset			
Ocular weakness	0/4 (0)	21/35 (60)	0.0372
Bulbar weakness	3/4 (75)	23/35 (65.7)	>0.9999
Limb weakness	1/4 (25)	6/35 (17.1)	>0.9999
Max disease severity (MGFA Clinical Classification)			
I	0/4 (0)	0/35 (0)	>0.9999
II	2/4 (50)	4/35 (11.4)	0.1045
III	2/4 (50)	12/35 (34.3)	0.6085
IV	0/4 (0)	8/35 (22.9)	0.5628
V	0/4 (0)	11/35 (31.4)	0.3091
Treatments received before IgA detection			
CS	4/4 (100)	NA	-
IS	2/4 (50)	NA	-
B-cell depletion	2/4 (50)	NA	-
Treatments during clinical course			
CS	4/4 (100)	34/35 (97.1)	>0.9999
IS	2/4 (50)	20/35 (57.1)	>0.9999
B cell depletion	3/4 (75)	24/35 (68.6)	>0.9999
Fc Rn inhibitors	1/4 (25)	0/35 (0)	0.0789
MGFA PIS at last follow up			
MM-or-better	1/4 (25)	16/35 (45.7)	0.6180
Improved	3/4 (75)	13/35 (37.1)	0.2684
Unchanged	0/4 (0)	3/35 (8.5)	>0.9999
Worse	0/4 (0)	1/35 (2.9)	>0.9999
Exacerbation	0/4 (0)	2/35 (5.7)	>0.9999
Median follow-up (IQR range), months	97.5 (20.5-225.5)	177.0 (78.0-242.0)	0.4275

Abbreviations: CS: corticosteroids; IQR: interquartile range; IS: immunosuppressive treatment; MGFA PIS: Myasthenia Gravis of America Post-Intervention Status; MM: minimal manifestations.
Fisher exact tests for categorical variables. Unpaired t tests for continuous variables.
The significance cutoff was set at $P < 0.05$.
*All *p* values for comparisons of characteristics between the two groups were nonsignificant.

Supplementary Table 3. Estimated frequency of circulating MuSK-specific IgA and IgG B cells isolated from three MuSK MG patients.

Patient ID	Number of CD27+ B cells screened	MuSK-specific IgA hits (wells)	Frequency of MuSK-specific IgA (%)	MuSK-specific IgG hits (wells)	Frequency of MuSK-specific IgG (%)	MuSK-specific IgA mAbs generated
MuSK-1(13)	30,000	3	0.01	5	0.016	1
MuSK-2(1)	86,700	1	0.001	1	0.001	1
MuSK-3(1)	17,000	2	0.012	5	0.029	1

$CD27^+$ B cells were isolated from three MuSK IgA-positive patients (MuSK-1, MuSK-2, MuSK-3). The number in parentheses following each patient ID indicates the timepoint of serial sample collection. After differentiation of B cells into antibody-secreting cells, immunoglobulin-rich supernatants were screened for MuSK IgA and MuSK IgG by cell-based assay to isolate MuSK-specific B cells. The B cells from those wells containing MuSK IgA antibodies were subcultured using a limiting dilution strategy to generate recombinant IgA monoclonal autoantibodies (see methods for additional details).

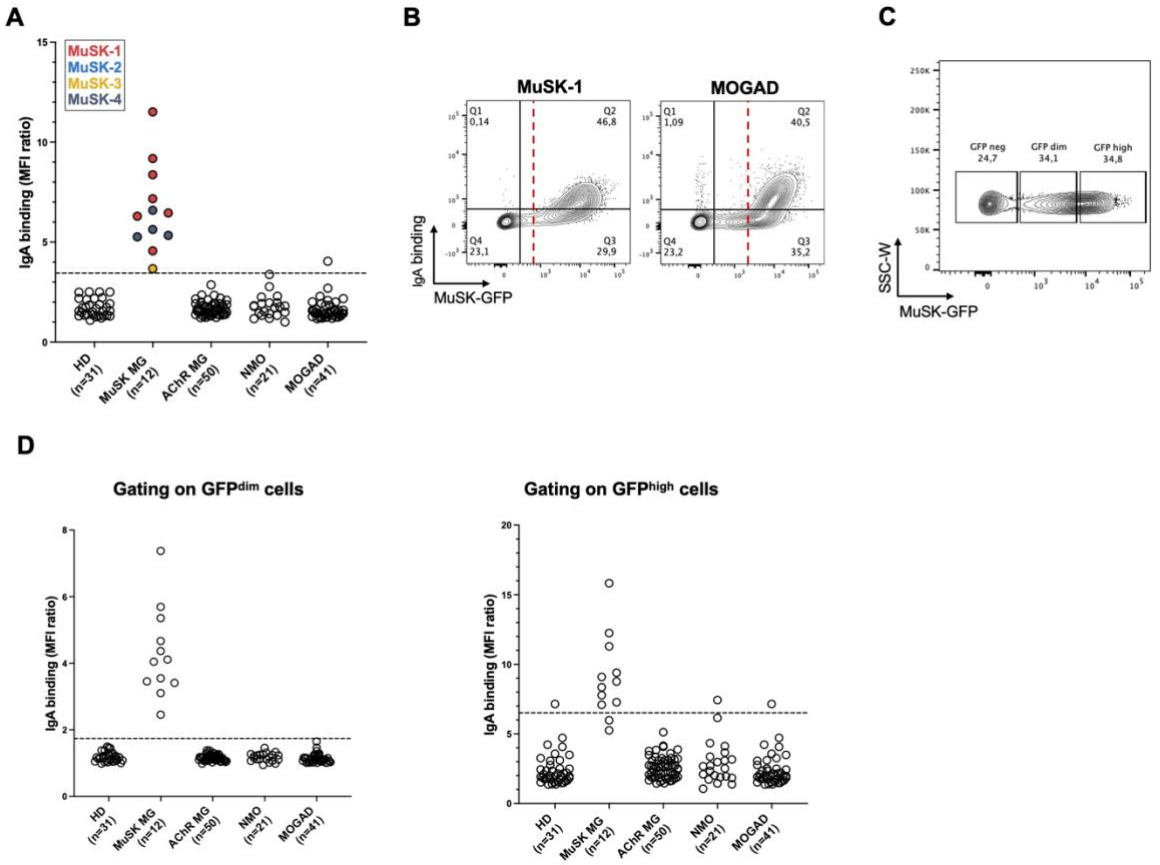

Supplementary Figure 1. MuSK IgA cell-based assay testing of patients with other neurological disorders. (A) Sera (n=112) from a cohort of patients with other neurological disorders (OND) — including AChR MG, neuromyelitis optica spectrum disorder, and myelin-oligodendrocyte glycoprotein-antibody associated disorder (MOGAD) — were tested for MuSK IgA Abs using flow cytometry. IgA binding was quantified as the ratio of the median Alexa Fluor 647 anti-IgA MFIs (median fluorescence intensity) in two cell populations: GFP-negative (no MuSK expression) and GFP-positive (MuSK expression). The cutoff for positivity (dashed line) was set at the mean MFI ratio of the HD group + four standard deviations. MuSK IgA Ab-positive sera (n=12) from four patients with MuSK MG (identified in the initial screening) were re-tested side-by-side with the OND samples. MuSK IgA positivity was confirmed in all 12 MuSK MG sera. One additional sample from a MOGAD patient tested positive for MuSK IgA Abs. **(B)** Flow cytometry plots of the MuSK IgA-positive MOGAD sample and a representative MuSK MG sample, with comparable IgA binding profiles (MFI ratios: 4.56 and 4.04, respectively). The red dashed lines indicate the IgA binding thresholds determined by visual inspection. The two samples differed in the onset of IgA binding, suggesting that recognition of MuSK-expressing cells by IgA Abs in the two samples requires different antigen concentrations. **(C)** A new gating strategy was tested based on two different MuSK cell densities, as determined by GFP expression (GFP^{dim} and GFP^{high}). **(D)** CBA results using GFP^{dim} and GFP^{high} MuSK-expressing cells. GFP^{dim} cells, corresponding to low-intermediate MuSK expression, discriminated MuSK MG sera from controls, whereas GFP^{high} cells did not. This difference in the MuSK expression level required for IgA binding may point to different Ab affinities in MuSK MG sera versus control sera.

A

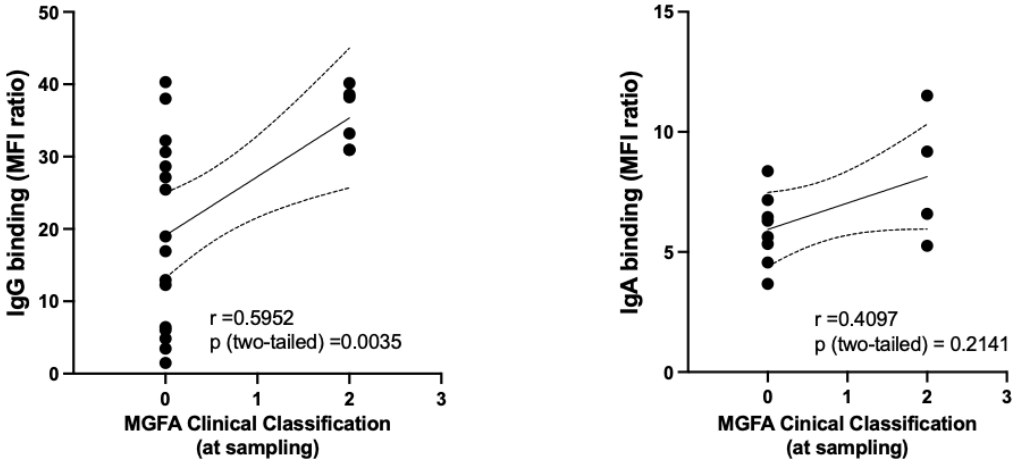

B

Tested sample	MuSK IgG4/IgA ratio
MuSK-3-1	**24.7**
MuSK-2-1	**9.1**
MuSK-1-9	**2.4**
MuSK-1-10	**8.6**
MuSK-1-11	**11.1**
MuSK-1-12	**0.5**
MuSK-1-13	**2.9**

Supplementary Figure 2. Correlation of MuSK IgG and IgA levels with clinical severity and estimation of absolute levels of MuSK autoantibodies. (A) Correlation between total MuSK IgG levels (left panel) and IgA levels (right panel) with clinical severity at sampling. Four MuSK IgA positive patients were included (each point represents a longitudinal serum sample). In each graph only samples showing MuSK IgG or IgA positivity were plotted. The correlation coefficient (r) and *p*-values were calculated using the Spearman's rank test. **(B)** Absolute levels of MuSK IgG4 and IgA Abs were estimated in representative sera (n=7). To enable antibody quantification, MuSK1B, a MuSK-specific mAb, was subcloned using two different backbones (IgG4 and IgA1). MuSK1B IgG4 and IgA1 mAbs were used to generate standard curves in each assay and allow quantification of absolute levels of the respective subclass. The ratio between MuSK IgG4 and IgA absolute levels is shown for each sample.
MFI: median fluorescence intensity; MGFA: Myasthenia Gravis Foundation of America.

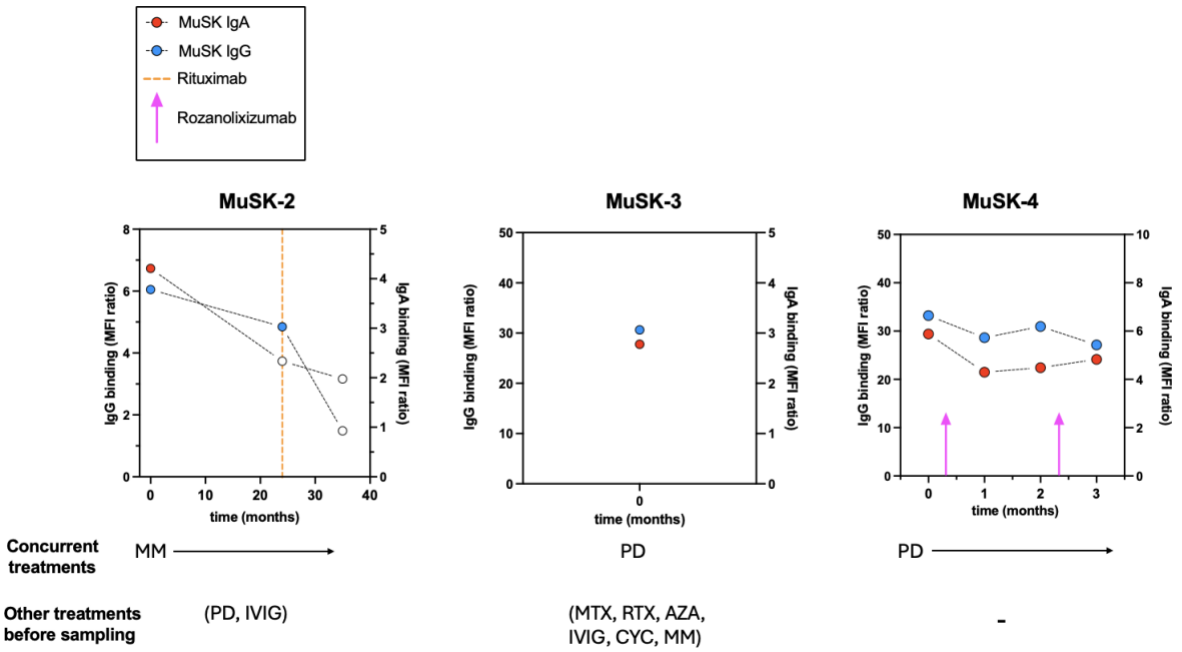

Supplementary Figure 3. Longitudinal tracking of MuSK IgG and IgA levels in patients with MuSK MG. Longitudinal tracking of serum MuSK IgG (blue dots) and IgA (red dots) levels in three patients (MuSK-2, MuSK-3 and MuSK-4). Longitudinal tracking of MuSK IgG and IgA in patient MuSK-1 is shown in **Figure 1**. For MuSK-3 only one sample was available. Full circles represent serum samples above the positivity cutoff, while empty circles indicate those below the cutoff. Treatments are indicated in the figure legends and below each graph. Abbreviations: AZA: azathioprine; CYC: cyclosporine; IVIG: intravenous immunoglobulin; MM: mycophenolate mofetil; MTX: methotrexate; PD: prednisone, RTX: rituximab.

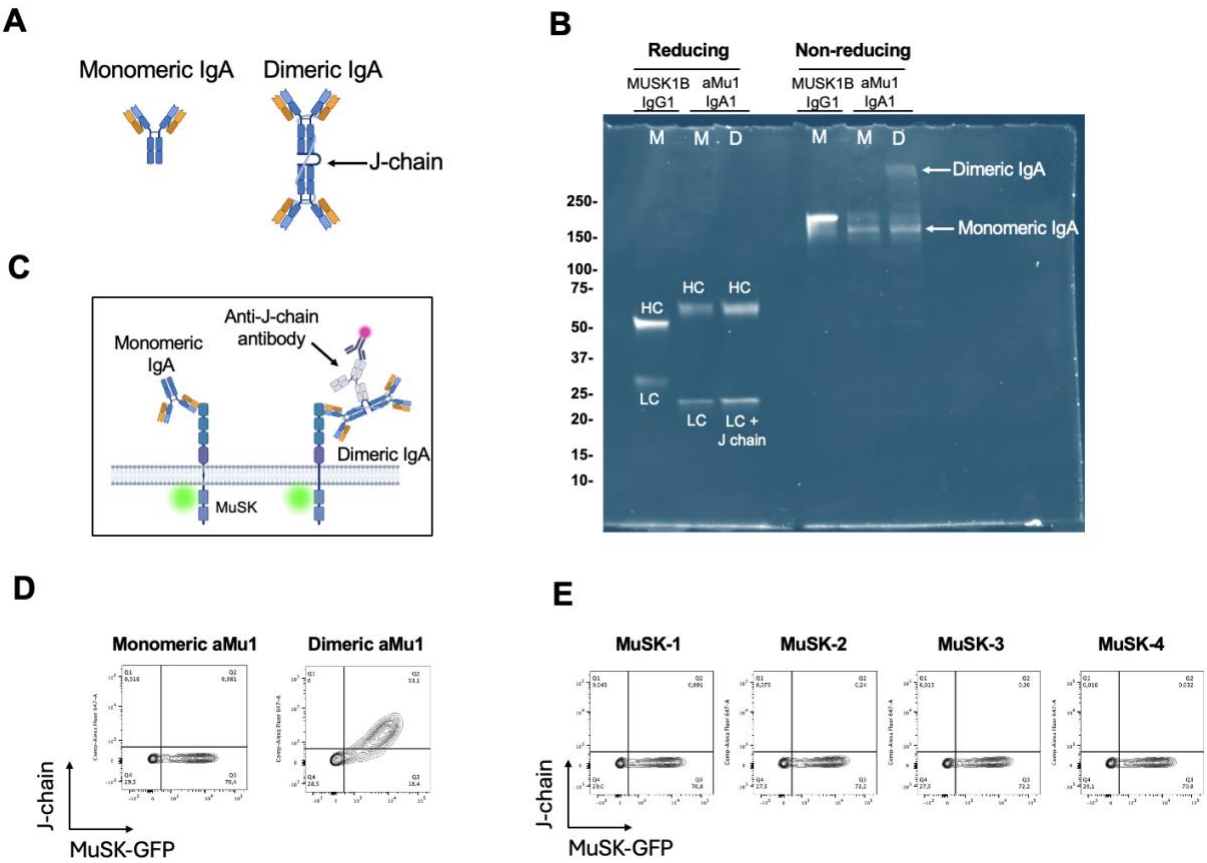

Supplementary Figure 4. Development of a cell-based assay for J-chain detection. (A) IgA antibodies exist as monomers and dimers. The J chain links monomeric IgA antibodies to form dimers. (**B**) SDS–PAGE under reducing and non-reducing conditions showing the assembly and purity of two MuSK-specific mAbs (MuSK1B IgG1 and aMu1 IgA1). Monomeric and dimeric forms of aMu1, an IgA-specific MuSK mAb, were expressed (a J-chain-encoding plasmid was co-transfected to enable dimerization; see Methods for additional details). HC, heavy chain; LC, light chain; J chain: joining chain; M: monomer; D: dimer. The J chain migrates at the same molecular weight as the light chain. Under non-reducing condition the IgA mAb expressed together with a J-chain plasmid (dimeric aMu1) appears as a mixture of monomers and dimers. **(C)** Schematic illustrating the design of a cell-based assay for J-chain detection. MuSK-expressing cells were incubated with either serum or mAbs, followed by the addition of a mouse anti-J chain antibody. Ab binding was detected with a fluorophore-conjugated secondary antibody. **(D)** This assay successfully discriminated between monomeric and dimeric forms of aMu1 IgA based on J-chain detection. **(E)** Flow plots of MuSK IgA Ab-positive sera from four patients. All sera were J-chain negative, suggesting that the majority of MuSK IgA Abs are monomeric. Created in BioRender. Masi, G. (2025) https://BioRender.com/08ex42b

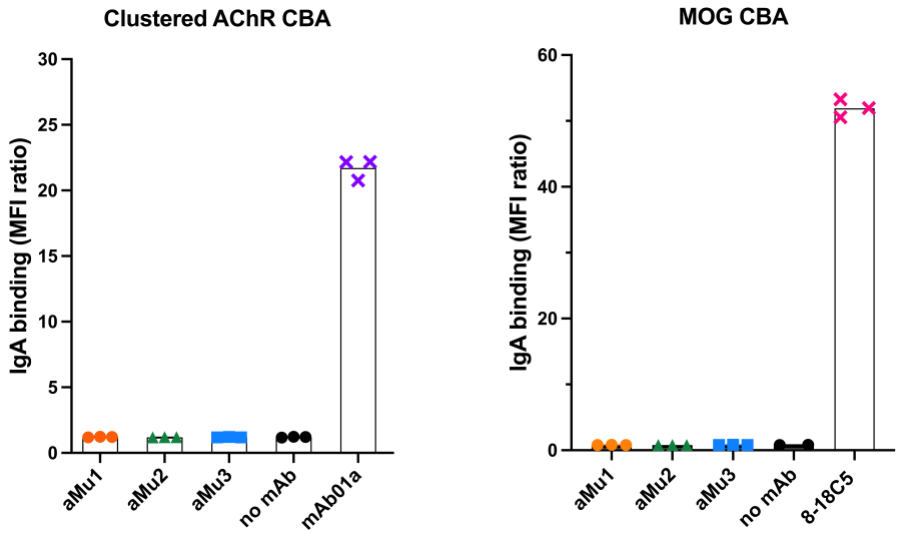

Supplementary Figure 5. Absence of cross-reactivity of three MuSK IgA mAbs against two neurological autoantigens. The three IgA mAbs (aMu1, aMu2 and aMu3) were tested for binding to the clustered acethlycholine receptor (AChR) (left graph) and myelin oligodendrocyte glycoprotein (MOG) (right graph) by live cell-based assay using flow cytometry. For each assay, a positive control mAb subcloned in an IgA1 vector was used (mAb01a, a mAb binding to AChR, and 8-18C5 which is specific for MOG).

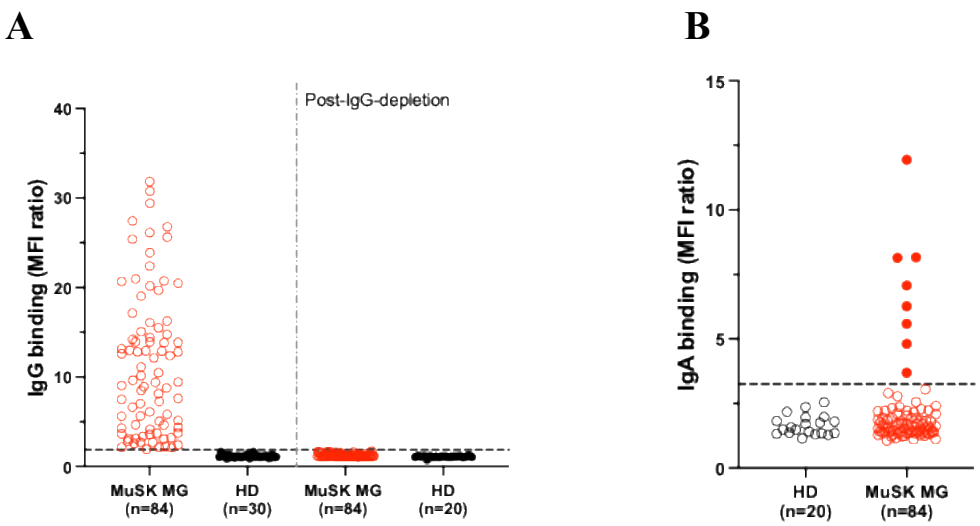

Supplementary Figure 6. **MuSK IgA cell-based assay testing following IgG depletion.** (**A**) MuSK IgG-positive sera from the discovery cohort (n=84) underwent two consecutive rounds of IgG depletion and were retested by CBA to confirm successful removal of MuSK IgG Abs. (**B**) The IgG-negative fractions were then screened for MuSK IgA Abs. This experiment showed eight samples harboring MuSK IgA Abs, corresponding to the eight MuSK IgA-positive sera identified in the initial screening.

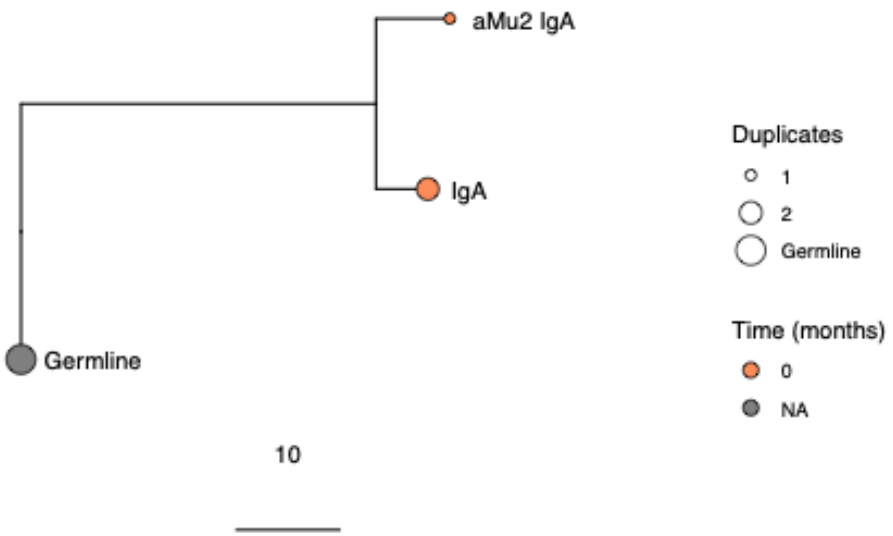

Supplementary Figure 7. Identification of a MuSK IgA clonal variant using high-throughput B-cell receptor sequencing. Clonal lineage tree containing BCR sequences from bulk RNA sequencing of serial samples from patient MuSK-2 from whom aMu2 was cloned. A maximum likelihood tree of aMu2 is shown, with 1 IgA CVs. Edge lengths represent the expected number of intervening somatic mutations between nodes (see scale bar). Colors correspond to the collection time point (months) at which each sequence was identified in relation to the first available collection timepoint. Duplicate sequences or those differing only by ambiguous nucleotides were collapsed, as indicated by the size of each tip.

A

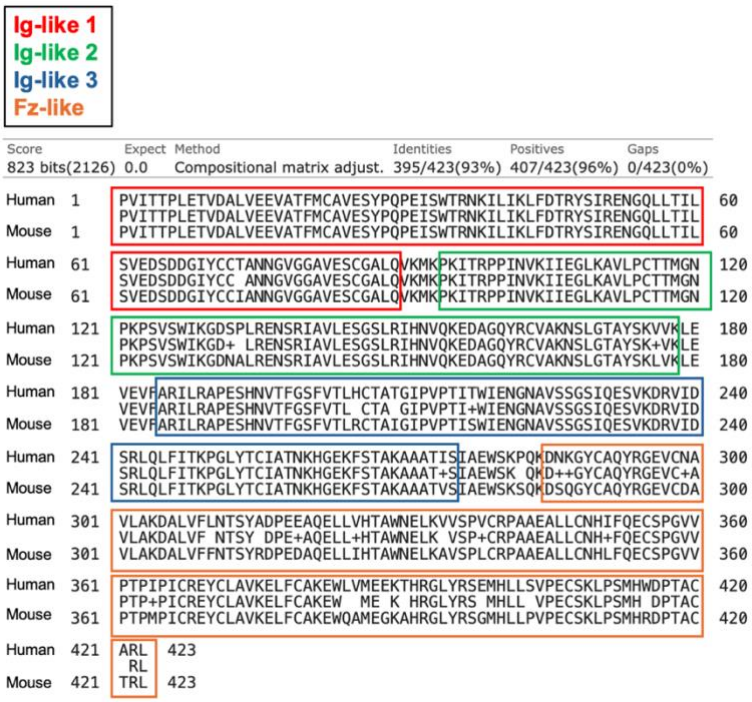

B

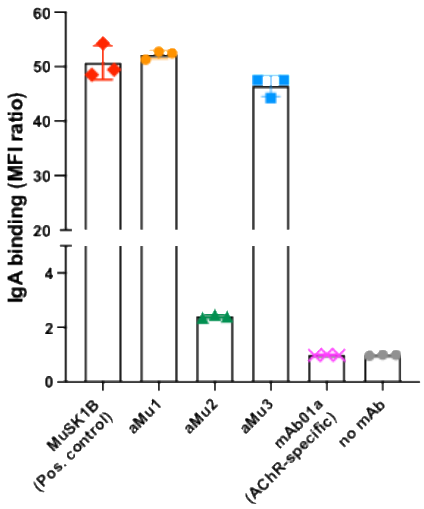

Supplementary Figure 8. Mouse MuSK cell-based testing results. (**A**) Sequence alignment of the human and murine MuSK ectodomain. MuSK domains are color-coded, as indicated by the figure legend. Sequence homology for the Ig-like 1 domain: 99%; Ig-like 2 domain: 96%; Ig-like 3 domain: 96%; Fz-like domain: 86%. (**B**) Three human-derived MuSK IgA mAbs (aMu1, aMu2 and aMu3) were tested for binding to mouse MuSK by live CBA. MuSK1B, a MuSK mAb known to cross-react with mouse MuSK, was used as a positive control. Compared to aMu1 and aMu3, aMu2 demonstrated minimal binding to mouse MuSK. All antibodies were expressed with an IgA1 backbone and tested at 1 μg/ml.

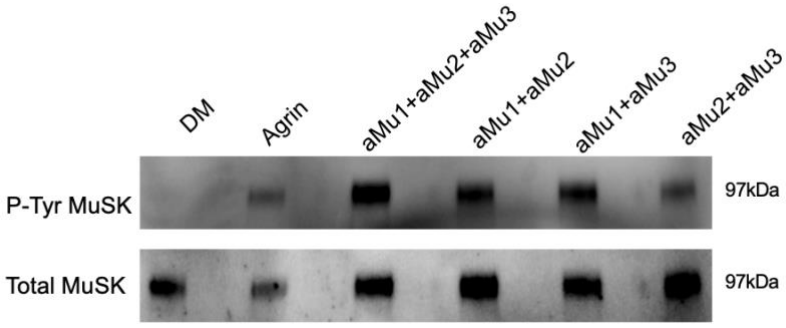

Supplementary Figure 9. Immunoblotting demonstrating phosphorylation of MuSK induced by the combination of MuSK-specific IgA mAbs. Different combinations of MuSK-specific IgA mAbs (aMu1, aMu2, aMu3) were incubated with C2C12 myotubes in the absence of agrin. MuSK phosphorylation (P-Tyr-MuSK) was assessed by immunoblotting. DM: differentiation media. See methods for additional details.

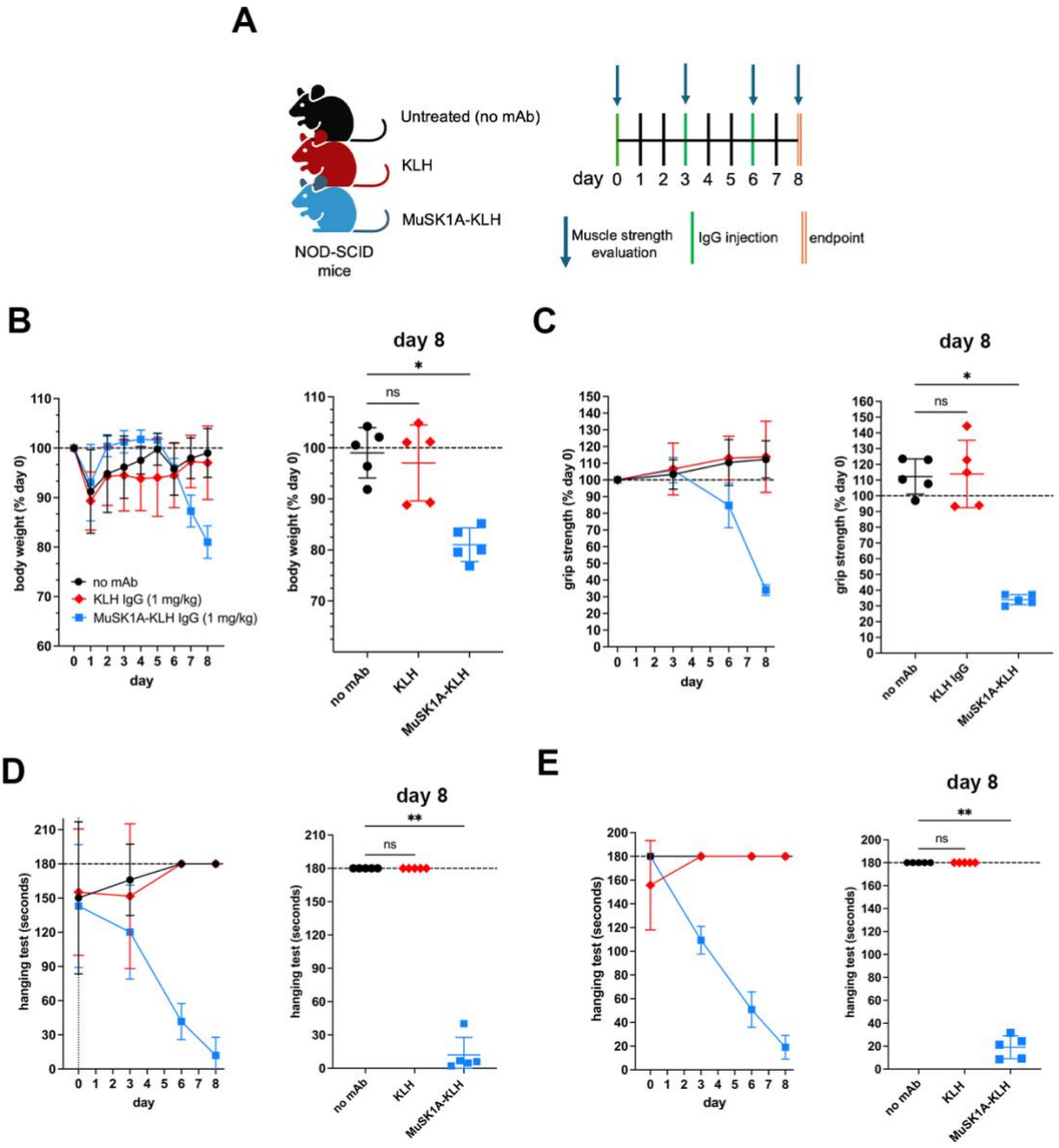

Supplementary Figure 10. Passive transfer of MuSK1A-KLH, a functionally monovalent MuSK-specific IgG mAb, causes myasthenic symptoms in NOD-SCID mice. **(A)** Experimental design of a passive immunization experiment with recombinant IgG mAbs. NOD-SCID mice (n=5 per group) received an intraperitoneal injection of either KLH IgG (control mAb) or MuSK1A-KLH IgG on day 0, 3 and 6 (mAb concentration: 1 mg/Kg). Body weight was measured daily. Two control groups (untreated mice and mice receiving KLH IgG mAb) were included in the experiment. **(B)** Left graph: body weight measurements. Right graph: body weight change on day 8 compared to baseline (day 0). **(C)** Grip strength measurements. Right graph: grip strength changes on day 8 compared to baseline (day 0). Rolling loop (**D**) and inverted mesh (**E**) hanging test results. Data on each panel show means and SDs. Multiple comparisons ANOVA (against untreated mice), Dunn's test; * $p<0.05$, ** $p<0.01$, *** $p<0.001$, **** $p<0.0001$, only shown when significant. Created in BioRender. Masi, G. (2025) https://BioRender.com/08ex42b

Supplementary Information for

IgA autoantibodies demonstrate a novel mechanism of MuSK myasthenia gravis pathology

Gianvito Masi[1,2,*], Kangzhi Chen[1,3], Alexandra C. Bayer[1,2], Rafael Bayarri-Olmos[2], Minh C. Pham[2], Annabel Wallace[4], Silvia Falso[5], Amelia Evoli[5], Raffaele Iorio[5], Kenneth B. Hoehn[6], Akiko Iwasaki[2,7,8], Richard J. Nowak[1], and Kevin C. O'Connor[1,2,*]

This PDF file includes:

- **Source data (unedited blot images)**

A

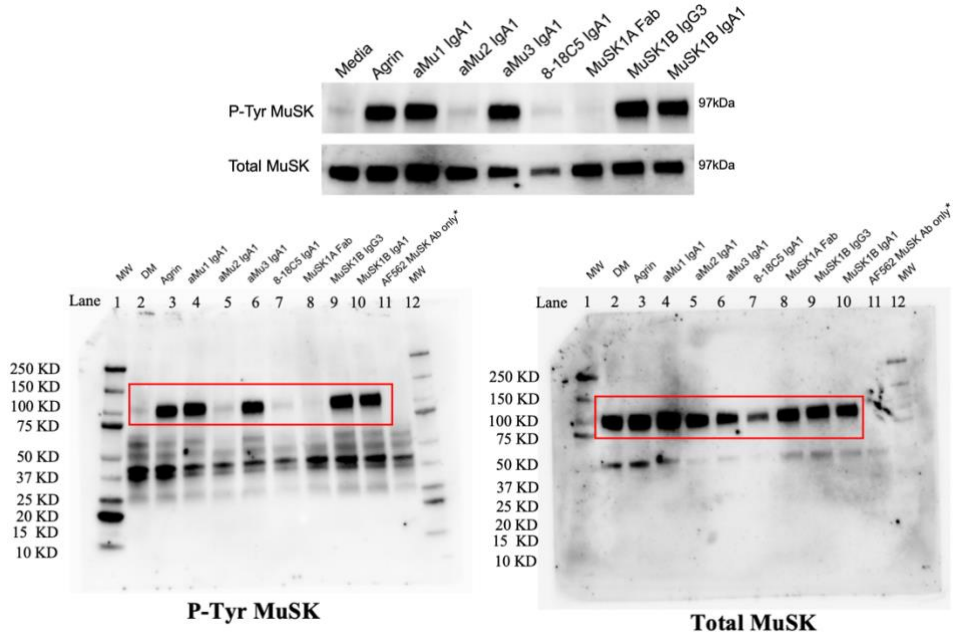

B

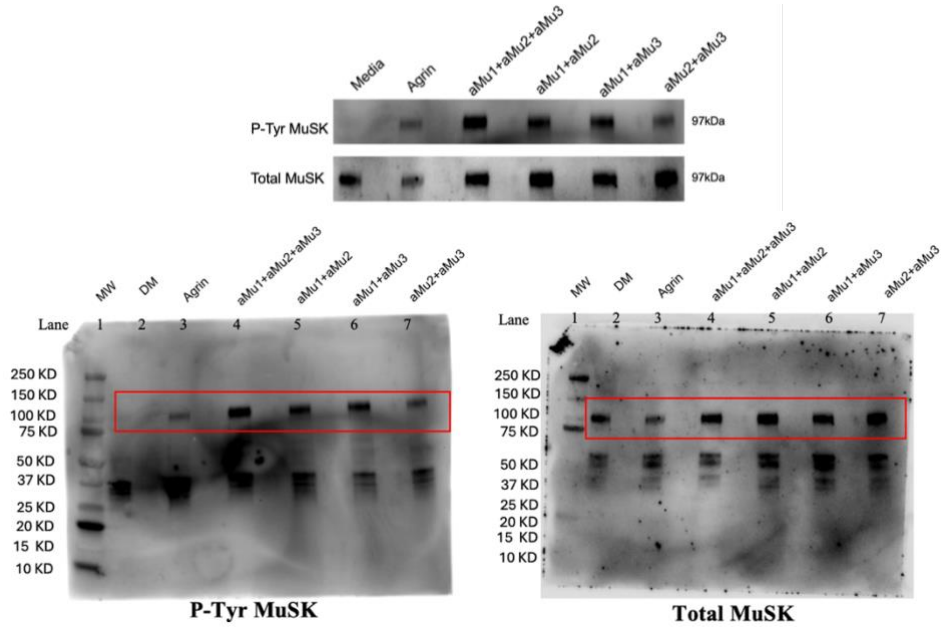

Source data (unedited blot images). Representative immunoblots showing phosphotyrosine bands and relative MuSK expression in C2C12 myotubes following incubation with differentiation media (DM), agrin, the three MuSK IgA mAbs (aMu1, aMu2, aMu3) or a mAb control (8-18C5 IgA). **(A)** Testing of individual mAbs in the absence of agrin. Several experimental controls were included (8-18C5 IgA, a mAb binding to the myelin oligodendrocyte glycoprotein; MuSK1A Fab, derived from an IgG4 MuSK-specific mAb; MuSK1B, a MuSK-specific mAb tested using an IgG3 (native) and IgA1 backbone). *Lane 12: AF562, a commercial MuSK-specific Ab used for IP, was tested alone (in the absence of C2C12 cells). **(B)** Testing of combinations of IgA MuSK-specific mAbs. Red rectangles indicate cropped areas used for **Figure 4B** and **Supplementary Figure 9.**